The protective roles of Eugenol on type 1 diabetes mellitus through NRF2 mediated oxidative stress pathway

Yalan Jiang[a, 1], Pingping He[a, 1], Ke Sheng[b, 1], Yongmiao Peng[b], Huilan Wu[b], Songwei Qian[e], Weiping Ji[e, f, *], Xiaoling Guo[a, b, c,d, *], Xiaoou Shan[a, c, d,*]

[a]*Department of Pediatrics, the Second Affiliated Hospital and Yuying Children's Hospital of Wenzhou Medical University, Wenzhou, Zhejiang 325027, China*

[b]*Basic Medical Research Center, the Second Affiliated Hospital and Yuying Children's Hospital of Wenzhou Medical University, Wenzhou, Zhejiang 325027, China*

[c]*Key Laboratory of Children Genitourinary Diseases of Wenzhou, the Second Affiliated Hospital and Yuying Children's Hospital of Wenzhou Medical University, Wenzhou, Zhejiang 325027, China*

[d]*Key Laboratory of Structural Malformations in Children of Zhejiang Province, the Second Affiliated Hospital and Yuying Children's Hospital of Wenzhou Medical University, Wenzhou, Zhejiang 325027, China*

[e]*Department of Genaral Surgery, the Quzhou Affiliated Hospital of Wenzhou Medical University，Quzhou People's Hospital, Quzhou, Zhejiang, China*

[f]*Department of General Surgery, the Second Affiliated Hospital and Yuying Children's Hospital of Wenzhou Medical University, Wenzhou, Zhejiang 325027, China*

**Correspondence: Weiping Ji, MD, Maoping Chu, MD, Xiaoling Guo, PhD, and Xiaoou Shan, MD, Basic Medical Research Center, the Second Affiliated Hospital and Yuying Children's Hospital of Wenzhou Medical University, 109 Xueyuan West Road, Wenzhou 325027, Zhejiang, China; Tel: 001-86-1375-886-0618; Fax: 86-0577-88002729; E-mail address: jiweiping@wmu.edu.cn, chmping@hotmail.com, guoxling@hotmail.com, seagullshan@wmu.edu.cn.*

[1]*These authors contributed equally to this work.*

Abstract

Type 1 diabetes mellitus (T1DM), known as insulin-dependent diabetes mellitus, is characterized by persistent hyperglycemia resulting from damage to the pancreatic β cells and an absolute deficiency of insulin, leading to multi-organ involvement and a poor prognosis. The progression of T1DM is significantly influenced by oxidative stress and apoptosis. The natural compound eugenol (EUG) possesses anti-inflammatory, anti-oxidant, and anti-apoptotic properties. However, the potential effects of EUG on T1DM had not been investigated. In this study, we established the streptozotocin (STZ)-induced T1DM mouse model *in vivo* and STZ-induced pancreatic β cell MIN6 cell model *in vitro* to investigate the protective effects of EUG on T1DM, and tried to elucidate its potential mechanism. Our findings demonstrated that the intervention of EUG could effectively induce the activation of nuclear factor E2-related factor 2 (NRF2), leading to an up-regulation in the expressions of downstream proteins NQO-1 and HO-1, which are regulated by NRF2. Moreover, this intervention exhibited a significant amelioration in pancreatic β cell damage associated with T1DM, accompanied by an elevation in insulin secretion and a reduction in the expression levels of apoptosis and oxidative stress related markers. Furthermore, ML385, an NRF2 inhibitor, reversed these effects of EUG. The present study suggested that EUG exerted protective effects on pancreatic β cells in T1DM by attenuating apoptosis and oxidative stress through the activation of the NRF2 signaling pathway. Consequently, EUG holds great promise as a potential therapeutic candidate for T1DM.

Keywords: Type 1 diabetes mellitus (T1DM), Eugenol (EUG), Oxidative stress, Apoptosis, Pancreatic β cell, NRF2 signaling pathway

1. Introduction

Type 1 diabetes mellitus (T1DM) is a chronic and progressive auto-immune disorder characterized by severe destruction of pancreatic β cells, leading to an absolute deficiency of insulin and subsequent hyperglycemia [1]. The symptoms of this disease include polydipsia, polyphagia, polyuria, wasting, etc., which can progress to ketoacidosis and even result in death without any treatment [2]. Additionally, chronic hyperglycemia can cause various complications, including diabetic nephropathy [3] and diabetic cardiomyopathy [4], which impose huge social and economic burdens. The global incidence of T1DM is rapidly increasing. According to the International Diabetes Federation (IDF), it is estimated that there were approximately 537 million adults (aged 20-79) worldwide affected by diabetes in 2021, while over 1.2 million children and adolescents (aged 0-19) were diagnosed with T1DM. The global prevalence of diabetes is projected to reach approximately 783 million individuals by 2045, with developing countries experiencing the largest increase [5]. Currently, insulin intervention remains the most efficacious approach for managing T1DM. However, challenges persist in addressing postprandial glycemic fluctuations [6] and life expectancy is shorter. Furthermore, in comparison to the general population, the quality of life is considerably compromised [7-9]. Therefore, it is crucial to explore more effective treatment strategies for T1DM patients.

Oxidative stress, a widely discussed concept in recent years, refers to the imbalance between oxygen free radical production and anti-oxidant reactions within cells, playing a crucial role in diabetes pathogenesis [10]. Hyperglycemia in diabetic patients can result in an augmented generation of reactive oxygen species (ROS) and the up-regulation of oxidative stress-related markers *in vivo*, while decreasing expression of anti-oxidant markers and disrupting internal homeostasis [11]. The cells typically possess robust mechanisms for anti-oxidant protection to maintain cellular homeostasis, particularly through the action of nuclear factor-E2-related factor 2 (NRF2), which serves as an efficient regulator of cellular anti-oxidant defense by modulating the expression of genes encoding anti-oxidant proteins [12]. NRF2 can interact with the Kelch-like ECH-associated protein 1 (KEAP1) in the cytoplasm

under normal physiological conditions, leading to subsequent degradation through ubiquitination. When cells are exposed to oxidative stress, NRF2 dissociates from KEAP1, evades ubiquitination, and translocates from the cytoplasm into the nucleus. Subsequently, it enhances the expression of target proteins, such as NAD(P)H quinone oxidoreductase-1 (NQO-1) and heme oxygenase-1 (HO-1) by binding to the anti-oxidant response element (ARE) [13-17]. Furthermore, ROS can induce DNA damage, and modulate the expression of proteins involved in cell regulation inhibition or activation, impair mitochondrial function, ultimately leading to apoptosis [18, 19]. Recent findings have indicated that the systemic activation of NRF2 signaling leads to a delay in the onset of T1DM in spontaneous non-obese diabetic (NOD) mice models [20]. Therefore, targeting NRF2 may offer potential for the prevention and treatment of T1DM.

Eugenol (EUG), a phenolic aromatic compound, is primarily derived from clove oil. The compound exhibits a range of biological activities, including anti-oxidant, anti-inflammatory, anti-apoptotic, and anti-bacterial effects [21]. Previous study has demonstrated that EUG could alleviate colitis by reducing oxidative stress through the activation of the KEAP1-NRF2 signaling pathway [22]. Additionally, EUG has been observed to attenuate apoptosis induced by transmissible gastroenteritis virus through the ROS-NRF2-ARE signaling pathway [23].

So far, no reports have been published to ascertain whether EUG confers a protective effect on damaged pancreatic β cells in individuals with T1DM. Our study aims to investigate the protective effect of EUG on pancreatic β cell damage in streptozotocin (STZ)-induced T1DM mouse model and STZ-induced MIN6 cell model, with the objective of elucidating the underlying mechanism. The findings may provide a potential novel therapeutic candidate drug for T1DM.

2. Results

2.1 Eugenol (EUG) can relieve the symptoms associate with type 1 diabetes mellitus (T1DM) and reduce the blood glucose level in T1DM mice

The experimental design timeline for *in vivo* experiments was depicted in Figure 1A. To assess the effects of EUG on T1DM mice, we recorded the fasting body weight (Figure 1B), fasting blood glucose levels (Figure 1C), water intake in 24 h (Figure 1D), food intake in 24 h (Figure 1E), and area of urine-soaked pads in T1DM mice (Supplement Figure 1A). These results showed that EUG effectively alleviated the multiple symptoms associated with T1DM, including polydipsia, hyperphagia, polyuria, and weight loss, while 20 mg/kg EUG exhibited the better improvement. At the termination of the experiment, the mice in each group showed distinct growth states (Supplement Figure 1B). The results demonstrated that the mice in T1DM group were smaller than the mice in Control group, and EUG treatment could improve this phenomenon. Given that T1DM can elevate the levels of urinary glucose and urine ketone, we conducted biochemical analysis for urine ketone and urine glucose (Supplement Figure 1C) in each group of mice. The results (Figure 1F and 1G) showed that administration of EUG exhibited a mitigating effect on the elevation of urine ketone and urinary glucose levels induced by T1DM.

It is widely acknowledged that oral glucose tolerance test (OGTT) can be used to detect T1DM and predict prognosis [24]. In this study, mice in each group were performed OGTT at week 1 (prior to T1DM induction), week 2 (two days after T1DM induction), week 3 (one week after T1DM induction), week 5 (three weeks after T1DM induction), and week 10 (at the end of the experiment). The findings demonstrated that treatment with EUG resulted in a reduction in blood glucose levels and improvement in islet function in T1DM mice (Figure 1H and 1I). The chronic and progressive nature of diabetes necessitates vigilance, as prolonged hyperglycemia can exert deleterious effects on vital organs such as the heart, kidneys, and liver [3, 4, 25]. Therefore, PAS staining was performed on the kidneys (Supplement Figure 1D). The results showed that T1DM indeed induced glycogen accumulation within the glomerulus, while EUG intervention showed reduction in such glycogen accumulation,

thereby enhancing the prognosis of T1DM. In brief, the administration of EUG could relieve the symptoms and reduce the blood glucose level in T1DM mice.

2.2 EUG can improve the damage degree of islets in T1DM mice

Insulin is produced by the β cells of pancreatic islets. Western blot (Figure 2A) and RT-qPCR were evaluated used to assess insulin expression levels in each group of mice. The quantitative results from both western blot (Figure 2B) and RT-qPCR (Figure 2C) showed that there was a decrease in insulin expression levels in T1DM mice, whereas EUG intervention increased the expression of insulin. In addition, the serum insulin levels of mice in each group were quantified using ELISA at different time points. The results showed a reduction in serum insulin levels after T1DM modeling, which were subsequently recovered by EUG intervention. Notably, the administration of 20 mg/kg EUG exhibited the better improvement effect (Figure 2D). The islets' structural integrity in each group of mice was performed through hematoxylin and eosin (H&E) staining. The results revealed that, in comparison to the Control group, the islet structure of T1DM mice exhibited severe damage with indistinct boundaries and evident vacuolization in the islet cells. EUG intervention demonstrated a potential for ameliorating the extent of islet damage (Figure 2E). Furthermore, insulin immunohistochemical staining was performed to further evaluate the expression of insulin in each group of mice (Figure 2F). The quantitative results showed a enhancement in insulin expression among T1DM mice following EUG treatment, and 20 mg/kg EUG displayed a better improvement (Figure 2G). These findings indicated that intervention with EUG could effectively ameliorate islet damage in T1DM mice.

2.3 EUG intervention alleviates T1DM by improving oxidative stress pathways

To investigate the potential molecular mechanisms underlying the regulation in T1DM, we performed RNA-seq analysis on pancreatic tissues obtained from the Control group, T1DM group, and EUG intervention group. The RNA-seq data revealed that among differentially expressed genes (DEGs), 28 genes were

up-regulated, and 17 genes were down-regulated in the EUG group compared to the T1DM group (Supplement Figure 2A). Furthermore, a heat map was generated to visualize the relative abundance of these DEGs affected by T1DM (Supplement Figure 2B). The findings were consistent with previous results, which showed the intervention of EUG could enhance the functionality of islet β cells, augment insulin secretion, and mitigate hyperglycemia in T1DM mice. GSEA analysis based on BP (biological process) gene revealed that compared to the T1DM group, the EUG intervention group exhibited significant enrichment in pathways, including "response to glucose," "response to carbohydrate," "cellular glucose homeostasis," and "positive regulation of insulin secretion" with NES 0 (Supplement Figure 2C-2F). These findings confirmed our previous experimental results and suggested a beneficial effect of EUG intervention on T1DM. To explore the therapeutic mechanism of EUG further, GSEA analysis based on MF (Molecular Function) gene set was performed. The results demonstrated that compared to the T1DM group, the EUG group showed significant enrichment and negative regulation in pathways related to "hydrogen peroxide-mediated programmed cell death" and "cell response to hydrogen peroxide" with NES < 0 (Supplement Figure 2G and 2H). Therefore, we concluded that EUG may alleviate T1DM by improving oxidative stress pathway.

2.4 EUG protects pancreatic β cells in T1DM mice by activating the NRF2 signaling pathway

Oxidative stress as a prominent pathogenic mechanism in T1DM is widely recognized [26]. In addition, the EUG compound has been reported to possess potent anti-oxidant properties and effectively activate the nuclear factor E2-related factor 2 (NRF2) [27]. Western blot was used to detect the expression levels of total NRF2 protein (T-NRF2) and nuclear NRF2 protein (N-NRF2) in each group of mice (Figure 3A). The findings showed that, in comparison to the Control group, intervention with EUG could activate NRF2, exerting anti-oxidative effects (Figure 3B). The result of RT-qPCR was consistent with those of western blot (Figure 3C). Furthermore, western blot was conducted to evaluate the expression of key proteins involved in the NRF2 signaling

pathway in each group of mice, including Kelch-like ECH-associated protein 1 (KEAP1), heme oxygenase-1 (HO-1), and NAD(P)H quinone dehydrogenase 1(NQO-1) (Figure 3D). The results showed that the intervention of EUG led to an up-regulation in protein expression levels of HO-1 and NQO-1, while a down-regulation in KEAP1 expression was observed due to the activation of the NRF2 signaling pathway (Figure 3E). The results of *Keap1*, *Nqo-1,* and *Ho-1* gene expression were consistent with aforementioned protein expression (Figure 3F). Finally, biochemical assays were conducted to measure the activities of serum oxidative stress-related markers scuh as Malondialdehyde (MDA), Superoxide dismutase (SOD), Catalase (CAT), and Glutathione peroxidase (GSH-Px) in each group of mice. The oxidative stress related index (MDA) was found to be elevated in the T1DM group, while the expression of anti-oxidant stress related indexes (SOD, CAT, and GSH-Px) were increased in the EUG intervention group (Figure 3G). These data suggested that EUG has the potential to alleviate oxidative stress-induced damage to pancreatic β cells in TIDM mice through activating the NRF2 signaling pathway.

2.5 EUG can reduce the apoptosis of pancreatic β cells in T1DM mice

DNA is essential for cell survival, and γH2AX serves as a dependable biomarker for detecting DNA damage [28]. Western blot was performed to assess the expression of γH2AX in each group of mice (Figure 4A). The result showed that the pancreatic β cells of T1DM mice exhibited DNA damage, and intervention with EUG was found to reduce the extent of DNA damages (Figure 4B). γH2AX immunohistochemical staining was also performed to assess γH2AX expression in each group of mice (Figure 4C). The quantitative finding was consistent with the western blot (Figure 4D).

It is well known that DNA damage in cells is closely associated with apoptosis. The potential anti-apoptotic effects of EUG on mouse pancreatic β cells were investigated by conducting a western blot to assess the expression levels of BCL2, BAX, and Cleaved Caspase-3 in the pancreatic β cells of mice in each experimental

group (Figure 5A). The results demonstrated that there was a increase in the number of apoptotic pancreatic β cells in T1DM mice compared to Control group. Moreover, EUG intervention effectively suppressed the apoptosis of pancreatic β cells in T1DM mice as well as 20 mg/kg EUG had the better effects (Figure 5B). Furthermore, the expression levels of *Bcl2* and *Bax* genes in pancreatic β cells of mice in each group were detected by RT-qPCR. The results obtained from western blot were consistent with these findings (Figure 5C). Finally, TUNEL staining was further performed to evaluate the apoptosis of pancreatic β cells in each group of mice (Figure 5D). The quantitative result showed an elevated count of apoptotic pancreatic β cells in T1DM mice, which could be mitigated by EUG intervention (Figure 5E). These findings suggested that EUG exhibited a potential to attenuate apoptosis of pancreatic β cells in T1DM mice.

2.6 EUG can alleviate the impairment of streptozotocin (STZ)-induced MIN6 cells

To further explore the potential effects of EUG on T1DM, we established STZ-induced MIN6 cell model *in vitro*. The cytotoxicity of STZ on MIN6 cells was evaluated using the CCK-8 assay. The result showed a dose-dependent decrease in the viability of MIN6 cells after 24 hours of treatmen with various concentrations of STZ (0-8 mM), and the optimal concentration for STZ treatment was 1 mM (Supplement Figure 3A). In addition, the cytotoxicity of EUG on MIN6 cells was also assessed using the CCK-8 assay. The result showed that the cell viability was not significantly affected by EUG concentration within the range of 0-600 μM (Supplement Figure 3B). After being treated with various concentrations of EUG (0-400 μM) for 2 h, MIN6 cells were subjected to 1 mM STZ treatment. The result showed that pre-treatment with EUG could enhance the viability of MIN6 cells, and reached the optimum after 50 μM EUG treatment (Supplement Figure 3C). Optical microscopy observation revealed that compared to Control group, the number of cells in STZ group was significantly reduced and cell morphology was worse. The administration of EUG treatment could ameliorate the above phenomena, whereas the intervention of NRF2 inhibitor ML385 (10 μM) could aggravate the cell damage (Supplement Figure 3D).

The experimental design timeline for *in vitro* experiments was illustrated in Figure 6A. Given the potential impact of pancreatic β cell damage on insulin secretion, we conducted an assessment of insulin protein and gene expression levels in different groups. The expression levels of insulin protein and gene in each group were assessed using western blot (Figure 6B) and RT-qPCR. The results (Figure 6C and 6D) showed that insulin levels in the STZ-induced group were lower than those in the Control group. However, after EUG treatment, STZ-induced insulin levels in MIN6 cells were elevated, which could be reversed by the intervention of the NRF2 inhibitor ML385. Furthermore, the cell culture supernatant of each group was further collected for detecting insulin levels using ELISA, and the obtained result was consistent with the aforementioned findings (Figure 6E). These findings suggested that EUG has the potential to enhance the insulin secretion of STZ-induced MIN6 cells.

2.7 EUG reduces STZ-induced MIN6 cell damage through activating the NRF2 signaling pathway

In order to further investigate the potential mechanism of EUG on T1DM, ML385, the typical NRF2 antagonist, was employed to assess the expression of proteins related to the NRF2 pathway through western blot (Figure 6F and 7A). The quantitative results showed that the protein levels of T-NRF2/β-Actin and N-NRF2/Lamin B in MIN6 cells treated with EUG were higher than those in the Control group (Figure 6H). Furthermore, treatment with EUG also resulted in an elevation of HO-1 and NQO-1 protein levels, while simultaneously reducing the level of KEAP1 (Figure 7B). However, the administration of ML385 could effectively reverse the effects of EUG on STZ-induced MIN6 cells. The quantitative results demonstrated that the ratio of T-NRF2/β-Actin and N-NRF2/Lamin B decreased after ML385 treatment. Moreover, RT-qPCR (Figure 6I and 7C) and immunofluorescence staining (Figure 6G and 7D) were conducted to evaluate the expressions of HO-1 and NRF2 in MIN6 cells under different treatments, with the trends of results were consistent with those of obtained from western blot and RT-qPCR (Figure 6J and 7F).

In order to demonstrate the ability of EUG to alleviate the STZ-induced MIN6

cells *in vitro* by activating the NRF2 signaling pathway, we utilized the NRF2 inhibitor ML385 to assess oxidative stress among different groups. MitoSOX staining (Figure 7E) showed that EUG reduced mitochondrial reactive oxygen species (ROS) levels in STZ-induced MIN6 cells, whereas ML385 was found to weaken this effect (Figure 7G). In addition, the flow cytometry was used to detect the cell ROS levels in different groups (Figure 7H). The quantitative result showed that STZ could increase the level of cell ROS, but EUG intervention could reduce the cell ROS level in STZ-induced MIN6 cells. Similarly, ML385 could reverse EUG effect on STZ-induced MIN6 (Figure 7I). These data suggested that EUG has the potential to ameliorate oxidative stress-induced damage in MIN6 cells caused by activating the NRF2 signaling pathway.

2.8 EUG inhibited STZ-induced apoptosis of islet β cell MIN6

To further explore the potential of EUG in attenuating STZ-induced damage to MIN6 cells *in vitro* through activating of the NRF2 signaling pathway, we used NRF2 inhibitor ML385 to evaluate the apoptosis levels in MIN6 cells under different treatments. Western blot result of γH2AX (Figure 8A) revealed that STZ treatment induced a increase in DNA damage in MIN6 cells, while intervention with EUG effectively reduced the extent of DNA damage in MIN6 cells, and ML385 intervention could reversed this phenomenon. The co-administration of EUG and ML385 exhibited a comparatively attenuated effect (Figure 8B). The result of γH2AX cell immunofluorescence staining (Figure 8C) was in accordance with the findings observed through western blot (Figure 8D). Occurrence of oxidative stress can induce cellular apoptosis [19]. The expressions of apoptosis-related proteins, including BCL2, BAX, and Cleaved Caspase-3, were examined using western blot (Figure 9A). The results demonstrated a induction of apoptosis in STZ-induced MIN6 cells, while EUG intervention played an anti-apoptotic role and ML385 could reverse this phenomenon (Figure 9B). The RT-qPCR results of *Bcl2* and *Bax* were consistent with above findings (Figure 9C). Additionally, TUNEL staining (Figure 9D) and flow cytometry of apoptosis (Figure 9F) were performed, and the trends of results were also

consistent with the aforementioned results (Figure 9E and 9G).

Based on the above findings, we hypothesized that EUG possesses the capability to ameliorate functional impairment of islet β cells in T1DM by reducing oxidative stress and apoptosis through activating the NRF2 signaling pathway. The potential mechanism of EUG in T1DM was illustrated in Figure 10.

3. Discussion

The pathogenesis of type 1 diabetes mellitus (T1DM) involves the autoimmune destruction of pancreatic β cells, leading to an absolute deficiency in insulin secretion. Consequently, T1DM is more prevalent among adolescents [1]. Although subcutaneous insulin injection is the conventional clinical treatment for T1DM, it fails to improve life quality of patients. Therefore, there is an urgent to explore more efficacious therapies for T1DM. A large number of studies have demonstrated that oxidative stress and apoptosis play crucial roles in causing islet damage in T1DM [26, 29]. In this study, we aimed to investigate the protective effects of eugenol (EUG) on islet damage in both *in vivo* and *in vitro* models of T1DM, and tried to illuminate the underlying mechanism.

EUG is a phenolic compound, which is present in various aromatic plants, exhibits a wide range of pharmacological properties including anti-oxidant, anti-inflammatory, anti-cancer, and anti-bacterial activities [21]. The administration of EUG has been shown to effectively lower blood glucose levels, ameliorate insulin resistance [30], inhibit the activity of key diabetes-related enzymes in diabetic rats [31], and suppress the production of advanced glycosylation end products associated with diabetes [32]. Therefore, it is speculated that EUG may have a protective effect on diabetes. The meta-analysis conducted by Carvalho et al. investigated the impact of EUG treatment on hyperglycemic murine models [33]. The findings demonstrated that purified EUG effectively improved glucose levels, blood lipids, body weight, and restored anti-oxidant defense in diabetic animals. Moreover, EUG exhibited a reduction in markers associated with kidney damage in experimental diabetic animals. The purity of the EUG utilized in this study was 99.3%, and the results in this reaserch were consistent with the meta-analysis in Carvalho et al.. In this study, we will try to explore the protective effects of EUG on streptozotocin (STZ)-induced *in vitro* and *in vivo* T1DM models. Our *in vivo* results showed that administration of EUG could effectively ameliorate the T1DM symptoms such as polydipsia, polyphagia, polyuria, and weight loss. Additionally, it also alleviate ketonuria and glycosuria of T1DM mice. The islet damage in T1DM mice was mitigated, and

insulin secretion was enhanced, along with effective alleviation of hyperglycemia symptoms, due to the intervention of EUG. As a chronic disease, diabetes can affect multiple organs, including the kidney, liver, and heart [3, 4, 25]. In this study, PAS staining showed that EUG intervention could reduce glomerular glycogen accumulation and improved the prognosis in T1DM mice. Our *in vitro* data showed that treatment with EUG could ameliorate the functional impairment of MIN6 cells induced by STZ, leading to increase insulin secretion levels, and reduced apoptosis and reactive oxygen species (ROS) production. Therefore, it can be speculated that EUG has the potential to treat T1DM.

The individuals suffering from diabetes exhibit persistent hyperglycemia, resulting in the generation of ROS that can cause cellular damage through various mechanisms [34]. Mitochondria function serve as the primary source of ROS, and in cases of mitochondrial dysfunction, there is an augmented production of ROS within the mitochondrial respiratory chain [35]. The mitochondrial respiratory chain complex enzymes are impaired under persistent hyperglycemia, leading to the development of secondary complications in diabetes [36, 37]. Therefore, oxidative stress is widely recognized as a major factor in the pathogenesis of diabetes. Our RNA sequencing analyses showed that the oxidative stress signaling were highly activated in T1DM mice and improved after intervention with EUG. Similarly, our study showed an elevation in malondialdehyde (MDA) levels in T1DM mice. This biomarker is associated with oxidative stress that represents the end product of lipid peroxidation caused by free radicals [38]. Additionally, anti-oxidant enzymes superoxide dismutase (SOD), catalase (CAT), and glutathione peroxidase (GSH-Px) can facilitate the catabolism of superoxide and peroxides in order to protect the body from oxidative stress damage. In our study, there was a reduction in the levels of SOD, CAT, and GSH-Px in T1DM group *in vivo*, while intervention with EUG could inhibit MDA level and promote productions of SOD, CAT, and GSH-Px in T1DM mice. These anti-oxidant enzymes subsequently inhibited the oxidative stress response in T1DM mice by restricting the occurrence of free radical reactions. Mitochondria play a pivotal role in the regulation of oxidative stress. The results of MitoSOX fluorescence

staining and ROS flow cytometry *in vitro* results showed that there was a increase in mitochondrial ROS and intracellular total ROS levels in STZ-induced MIN6 cells, which could be attenuated by EUG intervention. Furthermore, both *in vivo* and *in vitro* findings have demonstrated that EUG exhibited the ability to augment the expression of the relevant indicators withth the NRF2 signaling pathway, which is associated with anti-oxidant stress response. To further verify the association between EUG and the NRF2 signaling pathway, the NRF2 specific inhibitor ML385 was used *in vitro* experiments [39]. Notably, ML385 could abolish the effects of EUG. Therefore, we hypothesized that the activation of NRF2 signaling pathway might function as a protective mechanism of EUG against STZ-induced T1DM.

NRF2 is a transcription factor that plays a crucial role in cellular response to oxidative stress by inducing the expression of various anti-oxidants [40], and its activity is regulated by the endogenous inhibitor KEAP1 [41]. The NRF2 and KEAP1 proteins form a conserved intracellular defense mechanism to combat oxidative stress. Normally, KEAP1-CUL3-E3 ubiquitin ligase typically targets the N-terminal Neh2 domain of NRF2, and then facilitates NRF2 ubiquitination, thereby maintaining a low level of NRF2 [42]. In response to oxidative stress, specific cysteine residues in KEAP1 are modified that induce conformational changes in the KEAP1-CUL3-E3 ubiquitin ligase complex, thereby disrupting NRF2 ubiquitination and facilitating its translocation into the nucleus for heterodimerization with small MAF protein (sMAF). This complex subsequently binds to anti-oxidant response elements (ARE) located in the promoter region of various cytoprotective genes, thereby facilitating their transcription and inducing the expression of a range of cell-protective genes, including NQO1, HO-1, SOD, CAT, GSH-Px. This process plays a crucial role in mitigating oxidative stress, exerting an anti-oxidative stress role [43]. Previous study had demonstrated that EUG could attenuate the oxidative stress and apoptosis induced by transmissible gastroenteritis virus through the ROS-NRF2-ARE signaling pathway [23]. To further explore the potential molecular mechanisms underlying the regulation in T1DM, we conducted RNA-seq analysis on pancreatic tissues obtained from the Control group, T1DM group, and EUG group. Our findings from DEGs and heat map

revealed the intervention of EUG could enhance the functionality of islet β cells, augment insulin secretion, and mitigate hyperglycemia in T1DM mice. GSEA analysis showed that compared to the T1DM group, the EUG intervention might alleviate T1DM by improving oxidative stress pathway. Additionally, in this study, both *in vivo* and *in vitro* data showed that EUG activated NRF2, promoting its translocation into the nucleus, and inducing the expression of cytoprotective proteins NQO-1 and HO-1. Moreover, *in vivo* study showed that NRF2 regulated the levels of anti-oxidant enzymes such as SOD, CAT, and GSH-Px to suppress free radical reactions, exerting a protective effect on T1DM mice. Our *in vivo* results suggested that EUG has the potential to alleviate pancreatic β cell damage by activating the NRF2 pathway, thereby augmenting insulin secretion and ameliorating the prognosis of T1DM. Meanwhile, the intervention of ML385 counteracted the anti-oxidant and anti-apoptotic effects of EUG, leading to a reduction in NRF2 nuclear translocation and down-regulation of anti-oxidant oxidases. Therefore, we hypothesized the activation of the NRF2 signaling pathway through EUG might potentially alleviate damage of pancreatic β cells in T1DM.

Mitochondria are the main sites for cellular production of ROS, and intracellular ROS can function as signaling molecules to regulate physiological functions withth the body. Accumulation of caused by hyperglycemia can result in a reduction in mitochondrial membrane potential and an increased in membrane permeability [44-46]. The apoptotic factor cytochrome C (Cyct) is released into the cytoplasm to initiate the activation of the Caspase cascade (e.g. Caspase9 and Caspase3 are activated successively), leading to chromosome aggregation and DNA fragmentation [47]. The protein Caspase-3, which is essential for cellular function, plays a pivotal role in the intricate process of programmed cell death known as apoptosis. The BCL-2 family proteins, encompassing anti-apoptotic proteins like BCL-2 and BCL-xl, as well as pro-apoptotic proteins such as BAX and BAD, can regulate this process [48]. The dysregulation of the BCL2/BAX, characterized by aberrant expression of anti-apoptotic or pro-apoptotic genes, can initiate apoptosis and ultimately result in organ damage [49]. The development of T1DM is attributed to the autoimmune

destruction of islet β cells, and islet activation stimulates antigen-presenting cells, triggering the activation of $CD4^+$ helper T cells and subsequent the release of chemokines/cytokines [50, 51]. The activation of CD8+ cytotoxic T cells is subsequently induced by these cytokines, resulting in the subsequent destruction of β cells. The apoptotic pathways of T1DM include exogenous (receptor mediated) and endogenous (mitochondria driven) mechanisms. Exogenous pathway encompasses $CD4^+$-$CD8^+$ interacting Fas pathway, while endogenous pathway is characterized by a delicate balance between anti-apoptotic B-cell lymphoma (BCL-2) and BCL-xL proteins with pro-apoptotic Bax, Bad, Bid, and Bik proteins [52]. Therefore, targeted intervention of apoptosis can effectively enhance the prognosis of T1DM. The EUG compound has been reported to alleviate precancerous breast lesions by inhibiting apoptosis through the HER2/PI3K-AKT pathway [53]. In this study, our *in vivo* and *in vitro* results showed that EUG treatment down-regulated the expression of BAX and Cleaved Caspase-3, while up-regulated the level of BCL2 in the T1DM mice. Additionally, it reduced the number of TUNEL positive cells, thereby exerting a protective effect on islet β cells in T1DM mice. The survival of cell is dependent on the integrity of DNA, as any damage to DNA has the potential to induce cellular apoptosis or necrosis [28]. In this study, our data demonstrated that the expression of the DNA damage biomarker γH2AX was elevated in T1DM group both *in vivo* and *in vitro*, whereas intervention with EUG could reversed this trend. The involvement of NRF2 in the regulation of apoptosis has been observed, and cells lacking NRF2 exhibit an increased occurrence of spontaneous apoptosis [54]. Our *in vitro* results showed that the NRF2 specific inhibitor ML385 could attenuate the anti-apoptosis effect of EUG on STZ-induced MIN6 cells. Consequently, we speculated that EUG exerts its apoptotic suppression through activating the NRF2 signaling pathway. The findings of this study suggest that EUG may exert a protective effect on pancreatic β cell damage in T1DM by mitigating oxidative stress and apoptosis through the activation of the NRF2 signaling pathway

In this study, *in vivo* and *in vitro* results suggested that EUG may exert a protective effect on pancreatic β cell damages in T1DM by alleviating oxidative stress

and apoptosis via activating the NRF2 signaling pathway. However, there are certain limitations to our study. Firstly, ML385 was solely used to assess the protective effect of EUG *in vitro* but not *in vivo*, and the inhibitory effect on NRF2 *in vivo* needs to be further investigated. Secondly, it is imperative to analyze the dynamics of NRF2 decay in order to ascertain whether EUG affects the stability of NRF2 protein and gain a deeper understanding of its mechanism of action. Lastly, although MIN6 cells are extensively utilized in diabetes *in vitro* research, the primary islet cells would be optimal for studying T1DM *in vitro*.

In conclusion, our studies have demonstrated that EUG treatment could alleviate the symptoms associate with T1DM and ameliorate the damage of islets in T1DM mice. Moreover, EUG exhibited the ability to attenuate the deleterious effects on MIN6 cells induced by STZ *in vitro*. Additionally, EUG exhibits inhibitory effects on the oxidative stress and apoptosis in T1DM group *in vivo* and *in vitro* by activating the NRF2 mediated oxidative stress pathway. These findings suggested that EUG holds potential as a therapeutic option for patients with TIDM.

4. Material and methods

4.1 Animal

The male C57BL/6 mice (n = 150) weighing 18~20 g and aged of 5~6-weeks were procured from Zhejiang Weitong Lihua Laboratory Animal Technology Co., LTD. The mice were housed in a temperature-controlled pathogen-free facility (SPF) environment with a light/dark cycle for 12 h, maintained at a temperature of 23°C ± 2°C, relative humidity between 45%-55%, and provided ad libitum accesse to food and water. All experimental operations were approved by the Ethics Committee of Laboratory Animals of Wenzhou Medical University, and were strictly adhered to the Guide for the Care and Use of Laboratory Animals.

4.2 Animal experiment

After one week of adaptive feeding, type 1 diabetes mellitus (T1DM) mouse model was established in C57BL/6 mice using streptozotocin (STZ; Sigma-Aldrich, CA, USA). Briefly, each morning after 5 h fasting period in each group of mice, STZ was dissolved in a 0.1 M sodium citrate buffer (Solarbio, China, Beijing), and then intraperitoneally injected into mice at a dose of 50 mg/kg for 5 consecutive days [55]. The STZ solution was prepared under dark conditions and utilized promptly due to its inherent instability and photosensitivity. The mice were administered a 10% glucose solution instead of water during T1DM modeling to prevent mortality resulting from transient hypoglycemia. Fasting blood glucose levels were measured three days after modeling, and mice with fasting glucose levels more than 250 mg/dL were included in the study.

The intervention treatment of T1DM mice is conducted through two methods: oral administration [56] and oral gavage [57-59]. Due to limited experimental conditions, it is not feasible to feed a single mouse in a single cage, which makes it challenging to precisely control the actual daily intervention dose for each mouse when using oral administration. To ensure that each mouse receives an intervention dose according to its weight and expected dosage, we employ a method of gavage. In addition, oral gavage is more convenient and easier to operate than oral

administration.

In terms of dosage setting for eugenol (EUG; purity > 98%, MedChemExpress, NJ, USA), previous studies have demonstrated that oral gavage of EUG (20mg/kg/day) is effective in improving hyperglycemic symptoms in mice for 15 weeks [60]. Additionally, studies have shown that oral gavage of EUG (5, 10 mg/kg/day) can cure visceral leishmaniasis in mice [61]. Based on these reports, the T1DM mice in our study were divided into five groups: Control (n = 30), T1DM (n = 30), T1DM + EUG (5 mg/kg/day) (n = 30), T1DM + EUG (10 mg/kg/day) (n = 30), and T1DM + EUG (20 mg/kg/day) (n = 30). Each group received daily oral gavage for 8 weeks, while the Control group received an equivalent volume of normal saline. Fasting blood glucose levels and fasting weight were measured and recorded on a weekly basis. Finally, serum samples were collected through orbital blood collection technique, while pancreatic tissue was isolated for subsequent experiments.

4.3 Fasting blood glucose, oral glucose tolerance test (OGTT)

The oral glucose tolerance test (OGTT) is widely regarded as the criterion for diagnosing T1DM, which is crucial methods for assessing pancreatic islet function [24]. Following a 14 h fasting period, the fasting blood glucose levels were measured in each group mice, and tail vein blood samples were collected and analyzed using a glucometer. OGTT was performed by administering a 20% glucose solution intragastrically after the fasting period, and blood glucose levels were measured at 0 min, 30 min, 60 min, 90 min, and 120 min following the initial gavage administration.

4.4 Food, water, urine volume, and urine glucose measurements

The changes in food and water intake for each group were recorded throughout the experiment by regulating the daily initial food intake (100 g) and water quantity (250 mL). After successful modeling of T1DM mice, the experimental animals were grouped based on method 4.2 as follows: Control, T1DM, T1DM + EUG (5 mg/kg/day), T1DM + EUG (10 mg/kg/day), and T1DM + EUG (20mg/kg/day). To ensure consistency among groups, each group consisted of five mice and had equal

amounts of diet (100 g), drinking water (250 mL), and environmental conditions for feeding. The urine volume of each cage was quantified by measuring the area of the bedding material saturated with urine. The urine samples from each group of mice were collected for the detection of urine glucose levels using the Urine Glucose Assay Kit (Jiancheng, Nanjing, Jiangsu, China).

4.5 Islet isolation

The method described by Xu et al. [62] was employed for the isolation of islets. Firstly, the common bile duct was ligated, and a retrograde injection of collagenase V solution (0.8 mg/mL; Sigma-Aldrich, CA, USA) was performed through the common bile duct until the pancreas was completely filled and foliated. The pancreas was then digested in 5 mL of collagenase V solution at a concentration of the same for 15 min at 37□ until the majority of pancreatic tissues were digested into chylous and silt. To stop the process of digestion, 10 mL of 4□ Hank's solution was added and then centrifuged after gentle shaking. The centrifugation was immediately stopped upon reaching a speed of 2000 rpm. The supernatant was discarded and the sediment was washed twice using Hank's balanced salt solution. Islet tissues were placed in 5 mL of 4□ Ficoll density gradient medium (1.119). After mixing, a sequence of slow drips consisting of 2 mL 4□ Ficoll density gradient medium (1.077) and 2 mL Hank's solution was performed before centrifugation at a speed of 2000 rpm for a duration of 5 min. The sediment was washed again with Hank's solution, and subsequently was picked under a dissecting microscope (Leica, Germany). The isolated islets were promptly utilized for subsequent experimental procedures.

4.6 Insulin and ketonuria enzyme-linked immunosorbent assay (ELISA)

After collecting the culture supernatant of MIN6 cells and mouse serum from each group, insulin levels in the samples were evaluated using a commercially available ELISA assay kit (Boyun, Shanghai, China) in accordance with the manufacturer's protocol. The urine samples from each group were collected for the quantification of ketonuria levels using a commercially available ELISA assay kit (Boyun, Shanghai,

China).

4.7 Periodic acid-schiff (PAS) staining

After dewaxing the paraffin sections, a periodic acid-schiff (PAS) staining kit (Servicebio, Wuhan, China) was utilized to detect glomerular glycogen accumulation. These tissue sections were immersed in a 0.5% periodate solution for 15 min, and subsequently stained with Schiff reagent for 30 min in darkness. Finally, the nuclei of these tissue sections were stained using hematoxylin reagent. The images of paraffin sections were captured using an optical microscope (Nikon, Japan).

4.8 Hematoxylin and eosin (H&E) staining

The fresh pancreatic tissues from mice in each group were carefully separated and promptly fixed with 4% paraformaldehyde (PFA; Solarbio, Beijing, China). After dehydration for 24 h, they were embedded in paraffin and sliced into 5 μm. Subsequently, the paraffin sections of pancreas were stained with hematoxylin and eosin (H&E) staining kit (Servicebio, Wuhan, China), and the pathological changes of pancreatic islets were observed under an optical microscope.

4.9 Immunohistochemistry staining

After dewaxing, the peroxidase blockade agent (Zsbio, Beijing, China) was applied to the tissue surface at room temperature (RT) for 20 min. Following a 15 min wash with PBS, sections were subjected to antigen repair by boiling in a pressure cooker containing 10 mM citrate acid buffer for 2 min (pH 6.0, Solarbio, Beijing, China). Subsequently, antigen blocking was performed using 10% goat serum (Beyotime, Shanghai, China), and then the slides were incubated with primary antibodies (listed in Supplementary Table 1) overnight at 4□. On the second day, these sections were incubated with goat anti-rabbit secondary antibody (1:2000, Affinity Biosciences) at 37□ for 2 h, and then stained with a solution of 3, 3' -diaminobenzidine DAB (Zsbio, Beijing, China) and hematoxylin. The images of pancreatic paraffin sections were captured using an optical microscope.

4.10. RNA-sequencing

Total RNAs were isolated using the Trizol Reagent (Invitrogen Life Technologies), after which the concentration, quality and integrity were determined using a NanoDrop spectrophotometer (Thermo Fisher Scientific, MA, USA). Products were purified (AMPure XP system) and quantified using the Agilent high sensitivity DNA assay on a Bioanalyzer 2100 system (Agilent). The sequencing library was then sequenced on NovaSeq 6000 platform (Illumina) by Shanghai Personal Biotechnology Cp. Ltd.

The DESeq package was used to analyze the differences in Gene expression profiles, and the gseGO function in the clusterProfiler package was used to conduct gene set enrichment analysis (GSEA) according to the Gene Ontology (GO) database. The analysis was performed in the R language environment (version 4.2.0). The gene expression data of the T1DM group and EUG intervention group were thoroughly preprocessed before analysis, including standardization, missing value processing and other necessary quality control steps. The pre-processed data were used to assess the enrichment of gene sets associated with GO in different biological states. The GO database used covers three main domains: biological processes (BP), molecular functions (MF), and cell components (CC). The significance level was set as $p < 0.05$ and NES score >1.4. The significance was corrected by multiple tests, and the *p*-value was adjusted by false discovery rate (FDR) method. The gseGO function was used to evaluate the enrichment of a gene set in a given gene expression data, including calculating the enrichment score (ES) and standardized enrichment score (NES) of the gene set.

4.11 Cell culture and treatment

The mouse pancreatic β cell line MIN6 was obtained from the American Type Culture Collection (ATCC, Manassas, VA, USA), and was cultured in Dulbecco's Modified Eagle Medium (DMEM; Gibco, United States) supplemented with 1% penicillin/streptomycin (P/S; Gibco, CA, USA), 10% fetal bovine serum (FBS; Gibco,

CA, USA), and 1% MEM NON-ESSENTIAL AMINO ACIDS SOLUTION (100×; NEAA, Gibco, USA) at a temperature of 37°C in a CO2 incubator with a concentration of 5%. The cells were passaged every three days.

The *in vitro* cell model of T1DM was induced by STZ. MIN6 cells were treated with various concentrations of STZ (0.5 mM, 1 mM, 2 mM, 4 mM, and 8 mM) for a duration of 24 h to determine the optimal working concentration. Subsequently, STZ-induced MIN6 cells were exposed to different concentrations of EUG (50 μM, 100 μM, 200 μM, 400 μM, and 600 μM) for a duration of 2 h to identify the optimal working concentration. Based on the optimal working concentrations of STZ and EUG respectively , we set different groups, including Control, STZ, STZ + EUG, STZ + ML385 (10 μM, MedChemExpress, NJ, USA), STZ + ML385 + EUG. Pre-treatment with either EUG or ML385 occurred 2 h prior to stimulation with STZ, simultaneous administration of ML385 and EUG mixture took place at the same time. Finally, the cells or cell supernatant from each respective group were collected for subsequent experiments.

4.12 Cell viability assay

The cell viability of MIN6 cells was assessed using the cell counting kit-8 (CCK-8, Yeasen, Shanghai, China) under different treatment conditions. MIN6 cells were seeded into 96-well plates at a density of 5×10^3/well. Once the cells reached 80%-90% confluence, they were subjected to treatment with different concentrations of drugs. The different doses of EUG were added into the 96-well plates 2 h prior to STZ treatment. Subsequent to drug administration, each well was supplemented with 100 μL DMEM containing 10 μL CCK-8 solution. After incubation at 37□ for 30 min, the absorbance at 450 nm in each well was quantified using a microplate reader (Thermo Fisher Scientific, MA, USA).

4.13 Western blot

The total proteins from mouse islets or MIN6 cells were obtained using RIPA lysis buffer (Solarbio, Beijing, China) supplemented with a phosphatase inhibitor (Solarbio,

Beijing, China) and a serine protease inhibitor (Solarbio, Beijing, China). Nuclear protein extraction was performed using the nuclear protein extraction kit (Beyotime, Shanghai, China), following the manufacturer's instructions. Protein concentration was determined using the BCA protein assay kit (Beyotime, Shanghai, China). The samples containing 20-80 μg of proteins were separated on 7.5% or 12.5% sodium dodecyl sulfate-polyacrylamide gels (SDS-PAGE), and subsequently transferred onto the polyvinylidene fluoride (PVDF) membranes (Thermo Fisher Scientific, MA USA). These membranes were then incubated with 8% skim milk (Beyotime, Shanghai, China) at RT for 3 h. After being washed with tris-buffered saline containing Tween-20 (TBST), these membranes were incubated overnight at 4□ with the primary antibodies listed in Supplementary Table 1. The membranes were then incubated with goat anti-mouse or goat anti-rabbit IgG HRP secondary antibodies (Affinity, Melbourne, Australia) diluted at a ratio of 1:5000 and kept at RT for 3 h. Finally, the protein bands were detected using the ECL chromogenic kit (EpiZyme, Shanghai, China), and visualized using the ChemiDic^{TM} XRS imaging system (Bio-Rad, CA USA). The intensity of protein bands was analyzed using Image J software (National Institutes of Health, MD, USA), which was normalized to β-Actin or Lamin B band.

4.14 Real–time quantitative polymerase chain reaction (RT–qPCR)

Total RNAs were extracted from mouse islets or MIN6 cells using Trizol reagent (Invitrogen, CA, USA). After measuring of RNA concentration by reading the OD value at 260 nm, cDNAs were synthesized from the RNAs using cDNA Synthesis SuperMix (TaKaRa, Kusatsu, Japan). RT-qPCR was then performed using SYBR Green SuperMix (TOYOBO, Osaka, Japan). Subsequently, cycle threshold (Ct) values were collected and normalized to *β-actin* levels. The mRNA levels were calculated using the $2^{(-\Delta\Delta Ct)}$ method. The primer sequences are provided in Supplementary Table 2.

4.15 Immunofluorescence staining

MIN6 cells in different groups were fixed with 4% PFA for 20 min. Then, they were

incubated with 0.3% Triton X-100 (Sigma-Aldrich, CA, USA) for 1 h, followed by incubation with 10% goat serum. After rinsing with PBS three times, the cells were incubated overnight at 4□ with the primary antibody (listed in Supplementary Table 1). Then, they were incubated with FITC-conjugated goat anti-rabbit IgG secondary antibody (1:100; Earthox, LA, USA) for 2 h at RT. Finally, the nuclei were stained using DAPI-containing anti-fluorescence quencher and observed under a fluorescence microscope (Nikon, Tokyo, Japan).

4.16 TUNEL staining

In vivo experiments, pancreatic paraffin sections were initially dewaxed in a 60°C oven, and then were incubated with protease K solution at 37°C for 30 min. Following PBS rinsing, the sections were stained with TUNEL mixture (Roche, Basel, Switzerland) at 37°C for 1 h in darkness. Then, DAB staining and hematoxylin staining were performed. Finally, the images of these sections were captured under an optical microscope.

In vitro experiments, the apoptosis of MIN6 cells in each group was assessed using the TUNEL apoptosis detection kit (Roche, Basel, Switzerland). Briefly, the cells were incubated with TUNEL reagent for 1 h at 37□ in dark environment , and subsequently washed with PBS before being stained with DAPI. Lastly, they were observed under a fluorescence microscope.

4.17 Annexin V and PI assay

The Annexin V FITC/PI apoptosis detection kit (Becton Dickinson, NJ, USA) was utilized for the assessment of apoptosis of MIN6 cells in different groups. Following collection and double washing with 4□ PBS, the cells were re-suspended in Binding Buffer. Subsequently, these cells were stained at RT with a mixture of 5 μL FITC Annexin V and 5 μL PI for a duration of 15 min in darkness. Finally, the quantification of cell apoptosis ratio was detected using the Flow Cytometer (Beckman, CA, USA).

4.18 Mitochondrial reactive oxygen species (ROS) detection

Mitochondrial ROS levels were evaluated using the MitoSOX Red mitochondrial superoxide indicator (Yeasen, Shanghai, China). The reagent was diluted with dimethyl sulfoxide (DMSO, Solarbio, Beijing, China). Subsequently, the MIN6 cells in each experimental group were incubated with MitoSOX reagent for 30 min at 37°C in dark environment. Finally, the nucleus was stained with an anti-fluorescence quencher containing DAPI, and images were captured under a fluorescence microscope.

4.19 Reactive oxygen species (ROS) detection

Intracellular levels of ROS were measured using the ROS assay kit (S0033S, Beyotime, Shanghai, China) on the basis of the manufacturer's instructions. In brief, MIN6 cells in each group were digested with trypsin which has no EDTA. Cells together with cell supernatants were incubated with diluted DCFH-DA solution at 37□ for 30 min in the dark. Finally labeled cells were detected by Flow Cytometer (Beckman Coulter, Breya, California, USA).

4.20 Statistical analysis

In this study, all data were expressed as mean ± SEM and analyzed by GraphPad Prism 9.0 (GraphPad Software Inc., CA, USA). All experiments were repeated at least three times independently. Statistical significance was analyzed by Student's *t*-test or one-way ANOVA followed by Turkey's multiple comparisons. The criterion for statistical significance was set at a *p*-value of less than 0.05.

Disclosure statement

The authors assert that they have no discernible conflicting financial interests.

Author contributions

Y. J. devised the experiments and conducted the majority of the study. Y.J. and X.G. drafted the manuscript. P.H. established the mice model and K.S. established the cell

culture system. Y.P., and H.W. prepared of reagents and materials. S.Q. analyzed the data. X.S., W.J., and X.G. contributed to critical revisions of the manuscript. The final version of the manuscript has been reviewed and approved by all authors.

Data availability

The RNA-Seq data were available in BioProject PRJNA1153736. Data supporting the present study can be obtained from the corresponding author upon reasonable request.

Funding

This work was supported by the Key Research and Development Program of Zhejiang Province (2023C03018), the Natural Science Foundation of Zhejiang Province (LY24H020008, LTGY23H030003, and TGY23H030014), the Major Science and Technology Special Project of Wenzhou (2018ZY018), the Public Welfare Science and Technology Plan Project of Wenzhou City (Y2020925 and Y20210174), and the Fourth Batch of Wenzhou Medical University 'Outstanding and Excellent Youth Training Project' (604090352/640).

Referrences:

[1] X. Lu, C. Zhao, Exercise and Type 1 Diabetes, Adv Exp Med Biol 1228 (2020) 107-121.

[2] F.Z. Syed, Type 1 Diabetes Mellitus, Ann Intern Med 175(3) (2022) Itc33-itc48.

[3] N. Papadopoulou-Marketou, S.A. Paschou, N. Marketos, S. Adamidi, S. Adamidis, C. Kanaka-Gantenbein, Diabetic nephropathy in type 1 diabetes, Minerva Med 109(3) (2018) 218-228.

[4] M. Wang, Y. Li, S. Li, J. Lv, Endothelial Dysfunction and Diabetic Cardiomyopathy, Front Endocrinol (Lausanne) 13 (2022) 851941.

[5] D.J. Magliano, E.J. Boyko, I.D.F.D.A.t.e.s. committee, IDF Diabetes Atlas, Idf diabetes atlas, International Diabetes Federation

© International Diabetes Federation, 2021., Brussels, 2021.

[6] E. Cobry, K. McFann, L. Messer, V. Gage, B. VanderWel, L. Horton, H.P. Chase,

Timing of meal insulin boluses to achieve optimal postprandial glycemic control in patients with type 1 diabetes, Diabetes Technol Ther 12(3) (2010) 173-7.

[7] E. Kalyva, E. Malakonaki, C. Eiser, D. Mamoulakis, Health-related quality of life (HRQoL) of children with type 1 diabetes mellitus (T1DM): self and parental perceptions, Pediatr Diabetes 12(1) (2011) 34-40.

[8] F.J. Cameron, C. Clarke, K. Hesketh, E.L. White, D.F. Boyce, V.L. Dalton, J. Cross, M. Brown, N.H. Thies, G. Pallas, P.W. Goss, G.A. Werther, Regional and urban Victorian diabetic youth: clinical and quality-of-life outcomes, J Paediatr Child Health 38(6) (2002) 593-6.

[9] R.G. Miller, A.M. Secrest, R.K. Sharma, T.J. Songer, T.J. Orchard, Improvements in the life expectancy of type 1 diabetes: the Pittsburgh Epidemiology of Diabetes Complications study cohort, Diabetes 61(11) (2012) 2987-92.

[10] J.L. Rains, S.K. Jain, Oxidative stress, insulin signaling, and diabetes, Free Radic Biol Med 50(5) (2011) 567-75.

[11] K. Maiese, S.D. Morhan, Z.Z. Chong, Oxidative stress biology and cell injury during type 1 and type 2 diabetes mellitus, Curr Neurovasc Res 4(1) (2007) 63-71.

[12] S. Sajadimajd, M. Khazaei, Oxidative Stress and Cancer: The Role of Nrf2, Curr Cancer Drug Targets 18(6) (2018) 538-557.

[13] A.T. Dinkova-Kostova, W.D. Holtzclaw, R.N. Cole, K. Itoh, N. Wakabayashi, Y. Katoh, M. Yamamoto, P. Talalay, Direct evidence that sulfhydryl groups of Keap1 are the sensors regulating induction of phase 2 enzymes that protect against carcinogens and oxidants, Proc Natl Acad Sci U S A 99(18) (2002) 11908-13.

[14] T. Nguyen, P. Nioi, C.B. Pickett, The Nrf2-antioxidant response element signaling pathway and its activation by oxidative stress, J Biol Chem 284(20) (2009) 13291-5.

[15] W.W. Wasserman, W.E. Fahl, Functional antioxidant responsive elements, Proc Natl Acad Sci U S A 94(10) (1997) 5361-6.

[16] D.D. Zhang, M. Hannink, Distinct cysteine residues in Keap1 are required for Keap1-dependent ubiquitination of Nrf2 and for stabilization of Nrf2 by chemopreventive agents and oxidative stress, Mol Cell Biol 23(22) (2003) 8137-51.

[17] H. Zhu, K. Itoh, M. Yamamoto, J.L. Zweier, Y. Li, Role of Nrf2 signaling in regulation of antioxidants and phase 2 enzymes in cardiac fibroblasts: protection against reactive oxygen and nitrogen species-induced cell injury, FEBS Lett 579(14) (2005) 3029-36.

[18] P.H. Aguiar, C. Furtado, B.M. Repolês, G.A. Ribeiro, I.C. Mendes, E.F. Peloso, F.R. Gadelha, A.M. Macedo, G.R. Franco, S.D. Pena, S.M. Teixeira, L.Q. Vieira, A.A. Guarneri, L.O. Andrade, C.R. Machado, Oxidative stress and DNA lesions: the role of 8-oxoguanine lesions in Trypanosoma cruzi cell viability, PLoS Negl Trop Dis 7(6) (2013) e2279.

[19] M. Liu, X. Wu, Y. Cui, P. Liu, B. Xiao, X. Zhang, J. Zhang, Z. Sun, M. Song, B. Shao, Y. Li, Mitophagy and apoptosis mediated by ROS participate in AlCl(3)-induced MC3T3-E1 cell dysfunction, Food Chem Toxicol 155 (2021) 112388.

[20] Y. Yagishita, A. Uruno, D.V. Chartoumpekis, T.W. Kensler, M. Yamamoto, Nrf2 represses the onset of type 1 diabetes in non-obese diabetic mice, J Endocrinol (2019).

[21] M. Ulanowska, B. Olas, Biological Properties and Prospects for the Application of Eugenol-A Review, Int J Mol Sci 22(7) (2021).

[22] S. Chen, X. Wu, S. Tang, J. Yin, Z. Song, X. He, Y. Yin, Eugenol Alleviates Dextran Sulfate Sodium-Induced Colitis Independent of Intestinal Microbiota in Mice, J Agric Food Chem 69(36) (2021) 10506-10514.

[23] K. Wang, Y. Tang, X. Wu, H. Liang, D. Chen, B. Yu, J. He, X. Mao, Z. Huang, H. Yan, A. Wu, Y. Luo, P. Zheng, J. Yu, H. Wang, J. Luo, Eugenol Attenuates Transmissible Gastroenteritis Virus-Induced Oxidative Stress and Apoptosis Via ROS-NRF2-ARE Signaling, Antioxidants (Basel) 11(9) (2022).

[24] O. Helminen, S. Aspholm, T. Pokka, J. Ilonen, O. Simell, R. Veijola, M. Knip, OGTT and random plasma glucose in the prediction of type 1 diabetes and time to diagnosis, Diabetologia 58(8) (2015) 1787-96.

[25] J. Khoury, Y. Zohar, N. Shehadeh, T. Saadi, Glycogenic hepatopathy, Hepatobiliary Pancreat Dis Int 17(2) (2018) 113-118.

[26] J.D. Piganelli, M.J. Mamula, E.A. James, The Role of β Cell Stress and Neo-Epitopes in the Immunopathology of Type 1 Diabetes, Front Endocrinol (Lausanne) 11 (2020) 624590.

[27] L. Ma, J. Liu, Q. Lin, Y. Gu, W. Yu, Eugenol protects cells against oxidative stress via Nrf2, Exp Ther Med 21(2) (2021) 107.

[28] A. Kinner, W. Wu, C. Staudt, G. Iliakis, Gamma-H2AX in recognition and signaling of DNA double-strand breaks in the context of chromatin, Nucleic Acids Res 36(17) (2008) 5678-94.

[29] I. Santin, D.L. Eizirik, Candidate genes for type 1 diabetes modulate pancreatic islet inflammation and β-cell apoptosis, Diabetes Obes Metab 15 Suppl 3 (2013) 71-81.

[30] B. Al-Trad, H. Alkhateeb, W. Alsmadi, M. Al-Zoubi, Eugenol ameliorates insulin resistance, oxidative stress and inflammation in high fat-diet/streptozotocin-induced diabetic rat, Life Sci 216 (2019) 183-188.

[31] K. Mnafgui, F. Kaanich, A. Derbali, K. Hamden, F. Derbali, S. Slama, N. Allouche, A. Elfeki, Inhibition of key enzymes related to diabetes and hypertension by Eugenol in vitro and in alloxan-induced diabetic rats, Arch Physiol Biochem 119(5) (2013) 225-33.

[32] P. Singh, R.H. Jayaramaiah, S.B. Agawane, G. Vannuruswamy, A.M. Korwar, A. Anand, V.S. Dhaygude, M.L. Shaikh, R.S. Joshi, R. Boppana, M.J. Kulkarni, H.V. Thulasiram, A.P. Giri, Potential Dual Role of Eugenol in Inhibiting Advanced Glycation End Products in Diabetes: Proteomic and Mechanistic Insights, Sci Rep 6 (2016) 18798.

[33] R.P.R. Carvalho, G.D.A. Lima, M. Machado-Neves, Effect of eugenol treatment in hyperglycemic murine models: A meta-analysis, Pharmacol Res 165 (2021) 105315.

[34] J. Chen, S.E. Stimpson, G.A. Fernandez-Bueno, C.E. Mathews, Mitochondrial Reactive Oxygen Species and Type 1 Diabetes, Antioxid Redox Signal 29(14) (2018) 1361-1372.

[35] S.R. Pieczenik, J. Neustadt, Mitochondrial dysfunction and molecular pathways

of disease, Exp Mol Pathol 83(1) (2007) 84-92.

[36] A.J. Kowaltowski, N.C. de Souza-Pinto, R.F. Castilho, A.E. Vercesi, Mitochondria and reactive oxygen species, Free Radic Biol Med 47(4) (2009) 333-43.

[37] P. Jezek, L. Hlavatá, Mitochondria in homeostasis of reactive oxygen species in cell, tissues, and organism, Int J Biochem Cell Biol 37(12) (2005) 2478-503.

[38] A. Ayala, M.F. Muñoz, S. Argüelles, Lipid peroxidation: production, metabolism, and signaling mechanisms of malondialdehyde and 4-hydroxy-2-nonenal, Oxid Med Cell Longev 2014 (2014) 360438.

[39] A. Singh, S. Venkannagari, K.H. Oh, Y.Q. Zhang, J.M. Rohde, L. Liu, S. Nimmagadda, K. Sudini, K.R. Brimacombe, S. Gajghate, J. Ma, A. Wang, X. Xu, S.A. Shahane, M. Xia, J. Woo, G.A. Mensah, Z. Wang, M. Ferrer, E. Gabrielson, Z. Li, F. Rastinejad, M. Shen, M.B. Boxer, S. Biswal, Small Molecule Inhibitor of NRF2 Selectively Intervenes Therapeutic Resistance in KEAP1-Deficient NSCLC Tumors, ACS Chem Biol 11(11) (2016) 3214-3225.

[40] Q.M. Chen, A.J. Maltagliati, Nrf2 at the heart of oxidative stress and cardiac protection, Physiol Genomics 50(2) (2018) 77-97.

[41] E. Kansanen, S.M. Kuosmanen, H. Leinonen, A.L. Levonen, The Keap1-Nrf2 pathway: Mechanisms of activation and dysregulation in cancer, Redox Biol 1(1) (2013) 45-9.

[42] P. Wang, J. Song, D. Ye, CRL3s: The BTB-CUL3-RING E3 Ubiquitin Ligases, Adv Exp Med Biol 1217 (2020) 211-223.

[43] C. Tonelli, I.I.C. Chio, D.A. Tuveson, Transcriptional Regulation by Nrf2, Antioxid Redox Signal 29(17) (2018) 1727-1745.

[44] H. Chen, X. Li, P.N. Epstein, MnSOD and catalase transgenes demonstrate that protection of islets from oxidative stress does not alter cytokine toxicity, Diabetes 54(5) (2005) 1437-46.

[45] D.A. Lepore, T.A. Shinkel, N. Fisicaro, T.B. Mysore, L.E. Johnson, A.J. d'Apice, P.J. Cowan, Enhanced expression of glutathione peroxidase protects islet beta cells from hypoxia-reoxygenation, Xenotransplantation 11(1) (2004) 53-9.

[46] L.I. Rachek, N.P. Thornley, V.I. Grishko, S.P. LeDoux, G.L. Wilson, Protection

of INS-1 cells from free fatty acid-induced apoptosis by targeting hOGG1 to mitochondria, Diabetes 55(4) (2006) 1022-8.

[47] M. D'Amelio, V. Cavallucci, F. Cecconi, Neuronal caspase-3 signaling: not only cell death, Cell Death Differ 17(7) (2010) 1104-14.

[48] J.M. Adams, S. Cory, The Bcl-2 protein family: arbiters of cell survival, Science 281(5381) (1998) 1322-6.

[49] J. Liao, F. Yang, Z. Tang, W. Yu, Q. Han, L. Hu, Y. Li, J. Guo, J. Pan, F. Ma, X. Ma, Y. Lin, Inhibition of Caspase-1-dependent pyroptosis attenuates copper-induced apoptosis in chicken hepatocytes, Ecotoxicol Environ Saf 174 (2019) 110-119.

[50] S. Tsai, A. Shameli, P. Santamaria, CD8+ T cells in type 1 diabetes, Adv Immunol 100 (2008) 79-124.

[51] E.A. James, R. Mallone, S.C. Kent, T.P. DiLorenzo, T-Cell Epitopes and Neo-epitopes in Type 1 Diabetes: A Comprehensive Update and Reappraisal, Diabetes 69(7) (2020) 1311-1335.

[52] T. Tomita, Apoptosis of pancreatic β-cells in Type 1 diabetes, Bosn J Basic Med Sci 17(3) (2017) 183-193.

[53] M.L. Abdullah, O. Al-Shabanah, Z.K. Hassan, M.M. Hafez, Eugenol-Induced Autophagy and Apoptosis in Breast Cancer Cells via PI3K/AKT/FOXO3a Pathway Inhibition, Int J Mol Sci 22(17) (2021).

[54] A.A. Merchant, A. Singh, W. Matsui, S. Biswal, The redox-sensitive transcription factor Nrf2 regulates murine hematopoietic stem cell survival independently of ROS levels, Blood 118(25) (2011) 6572-9.

[55] B.L. Furman, Streptozotocin-Induced Diabetic Models in Mice and Rats, Curr Protoc 1(4) (2021) e78.

[56] H. Zhao, H. Wu, M. Duan, R. Liu, Q. Zhu, K. Zhang, L. Wang, Cinnamaldehyde Improves Metabolic Functions in Streptozotocin-Induced Diabetic Mice by Regulating Gut Microbiota, Drug Des Devel Ther 15 (2021) 2339-2355.

[57] D. Xing, Q. Zhou, Y. Wang, J. Xu, Effects of Tauroursodeoxycholic Acid and 4-Phenylbutyric Acid on Selenium Distribution in Mice Model with Type 1 Diabetes, Biol Trace Elem Res 201(3) (2023) 1205-1213.

[58] S. Sudirman, C.S. Lai, Y.L. Yan, H.I. Yeh, Z.L. Kong, Histological evidence of chitosan-encapsulated curcumin suppresses heart and kidney damages on streptozotocin-induced type-1 diabetes in mice model, Sci Rep 9(1) (2019) 15233.

[59] H. Yao, H. Shi, C. Jiang, M. Fan, Y. Zhang, W. Qian, R. Lin, L-Fucose promotes enteric nervous system regeneration in type 1 diabetic mice by inhibiting SMAD2 signaling pathway in enteric neural precursor cells, Cell Commun Signal 21(1) (2023) 273.

[60] K.J. Jeong, D.Y. Kim, H.Y. Quan, H.K. Jo, G.W. Kim, S.H. Chung, Effects of eugenol on hepatic glucose production and AMPK signaling pathway in hepatocytes and C57BL/6J mice, Fitoterapia 93 (2014) 150-62.

[61] M.R. Charan Raja, A. Kar, S. Srinivasan, D. Chellappan, J. Debnath, S. Kar Mahapatra, Oral administration of eugenol oleate cures experimental visceral leishmaniasis through cytokines abundance, Cytokine 145 (2021) 155301.

[62] Y. Xu, H. Fu, Z. Wang, X. Zhou, Y. Xu, D. Wang, S. Xue, X. Li, [Improved methods of isolation and purification of rat islets and its viability research], Zhongguo Xiu Fu Chong Jian Wai Ke Za Zhi 24(4) (2010) 406-9.

Figure Legends

Figure. 1. The EUG treatment effectively alleviated symptoms associated with T1DM mice. (A) The schematic diagram depicts the progress of animal experiments in each group of mice. Different colors indicate different treatments for mice. (B) The fasting weight levels of mice were measured weekly in each group (n = 30 mice). (C) The fasting blood glucose levels of mice were measured weekly in each group (n = 30 mice). (D) The water intake/cage in each group of mice (n = 6 cages, 5 mice/cage). (E) The food intake/cage in each group of mice (n = 6 cages, 5 mice/cage). (F) Urine ketones in each group were detected by ELISA (n = 30 mice). (G) The urine glucose levels of mice was measured by biochemical test in each group of mice (n = 30 mice). (H) The curve graph of oral glucose tolerance test (OGTT) from 0 min to 120 min at week 1, week 2, week 3, week 5, and week 10 (n = 30 mice). (I) The quantitative results of OGTT at week 1, week 2, week 3, week 5, and week 10 (n = 30 mice).

Mean ± SEM. All experiments were repeated at least three times independently. Compare with the Control group $^{*}p < 0.05$, compare with the Control group $^{**}p < 0.01$ compare with the Control group $^{***}p < 0.001$, compare with the T1DM group $^{\#}p < 0.05$, compare with the T1DM group $^{\#\#}p < 0.01$, compare with the T1DM group $^{\#\#}p < 0.001$ indicate significant differences, and *ns* > 0.05 means no significance difference.

Figure. 2. EUG improved the pancreas islet structure and function in T1DM mice. (A) The detection of Insulin expression in different groups using western blot. (B) The quantification of western blot gel bands in different groups (n = 3 independently repeated experiments). (C) The gene levels of *Ins1* in different groups (n = 5 independently repeated experiments). (D) ELISA analysis of serum fasting insulin levels at different time points (n = 5 independently repeated experiments). (E) The representative H&E staining images of pancreatic paraffin sections in each group of mice. Scale bars 50 μm, 20 μm. (F) The representative immumohistochemical staining of Insulin in pancreas islet in each group of mice. Scale bars 50 μm, 20 μm. (G) The quantitative analysis of immumohistochemical staining (n = 5 independently repeated experiments). Mean ± SEM. $^{*}p < 0.05$, $^{**}p < 0.01$, $^{***}p < 0.001$ indicate significant differences, and *ns* > 0.05 means no significance difference.

Figure. 3. EUG attenuated excessive oxidative stress through activating NRF2 signaling pathway in T1DM mice. (A) The detection of T-NRF2, N-NRF2 expression in different groups using western blot. (B) The quantification of western blot gel bands in different groups (n = 3 independently repeated experiments). (C) The gene levels of *Nrf2* in different groups (n = 5 independently repeated experiments). (D) The detection of KEAP1, HO-1, and NQO-1 expression in different groups using western blot. (E) The quantification of western blot gel bands in different groups (n = 3 independently repeated experiments). (F) The gene levels of *Keap1*, *Nqo-1*, and *Ho-1* in different groups (n = 5 independently repeated experiments). (G) The levels of serum biochemical indexes (MDA, SOD, CAT, and GSH-Px) in each group of mice (n = 5 independently repeated experiments). Mean ± SEM. $^{*}p < 0.05$, $^{**}p < 0.01$, $^{***}p$

< 0.001 indicate significant differences, and *ns* > 0.05 means no significance difference.

Figure. 4. EUG decreased the expression level of γH2AX in T1DM mice. (A) The detection of γH2AX expression in different groups using western blot. (B) The quantification of western blot gel bands in different groups (n = 3 independently repeated experiments). (C) The representative immumohistochemical staining of γH2AX in pancreas islet in each group of mice. Black arrows were employed to highlight the presence of brown-stained islet β cells. Scale bars 100 μm, 25 μm. (D) The quantitative analysis of immumohistochemical staining (n = 5 independently repeated experiments). Mean ± SEM. $^{*}p < 0.05$, $^{**}p < 0.01$, $^{***}p < 0.001$ indicate significant differences, and *ns* > 0.05 means no significance difference.

Figure. 5. EUG reduced apoptosis of pancreatic β cells in T1DM mice. (A) The detection of BCL2, BAX, Cleaved Caspase-3 expression in different groups using western blot. (B) The quantification of western blot gel bands in different groups (n = 3 independently repeated experiments). (C) The gene levels of *Bax*, *Bcl2*, and *Bcl2/Bax* in different groups (n = 5 independently repeated experiments). (D) The immumohistochemical staining of TUNEL in pancreas islet in each group of mice. Scale bars 50 μm, 20 μm. (E) The quantification results of TUNEL staining in different groups (n = 5 independently repeated experiments). Mean ± SEM. $^{*}p < 0.05$, $^{**}p < 0.01$, $^{***}p < 0.001$ indicate significant differences, and *ns* > 0.05 means no significance difference.

Figure. 6. EUG improved STZ-induced MIN6 cells insulin secretion by facilitating NRF2 nuclear translocation *in vitro*. (A) The schematic diagram depicts the different interventions in cell experiments in MIN6 cells. (B) The detection of Insulin expression in different groups using western blot. (C) The quantification of western blot gel bands in different groups (n = 3 independently repeated experiments). (D) The gene levels of *Ins1* in different groups (n = 5 independently repeated

experiments). (E) ELISA analysis of serum insulin levels of MIN6 cell in different groups (n = 5 independently repeated experiments). (F) The detection of T-NRF2, N-NRF2 expression in different groups using western blot. (G) The representative immunofluorescence staining images of NRF2 (green) in each group of MIN6 cells. Nuclei were stained with DAPI (blue). Scale bar 10 μm. (H) The quantification of western blot gel bands in different groups (n = 3 independently repeated experiments) (I) The gene levels of *Nrf2* in different groups (n = 5 independently repeated experiments). (J) The quantification of immunofluorescence staining in different groups (n = 5 independently repeated experiments). Mean ± SEM. $^{*}p < 0.05$, $^{**}p < 0.01$, $^{***}p < 0.001$ indicate significant differences, and *ns* > 0.05 means no significance difference.

Figure. 7. EUG promoted the expression of NRF2 signaling pathway related proteins to reduce intracellular ROS level. (A) The detection of KEAP1, HO-1, and NQO-1 expression in different groups using western blot. (B) The quantification of western blot gel bands in different groups (n = 3 independently repeated experiments). (C) The gene levels of *Keap1*, *Nqo-1*, and *Ho-1* in different groups (n = 5 independently repeated experiments). (D) The representative immunofluorescence staining images of HO-1 (green) in each group of MIN6 cells. Nuclei were stained with DAPI (blue). Scale bar 10 μm. (E) The generation of mitochondrial ROS in each group was detected by MitoSOX (red) and DAPI (blue) staining. Scale bar 100 μm. (F) The quantification of immunofluorescence staining in different groups (n = 5 independently repeated experiments) (G) The quantitative analysis of immunofluorescence staining in different groups (n = 5 independently repeated experiments). (H) The cell ROS in each group was analyzed using flow cytometry after DCFH-DA staining. (I) The quantitative analysis of flow cytometry after DCFH-DA staining (n = 3 independently repeated experiments). Mean ± SEM. $^{*}p < 0.05$, $^{**}p < 0.01$, $^{***}p < 0.001$ indicate significant differences, and *ns* > 0.05 means no significance difference.

Figure. 8. EUG attenuated γH2AX expression in STZ-induced MIN6 cells *in vitro*. (A) The detection of γH2AX expression in different groups using western blot. (B) The quantification of western blot gel bands in different groups (n = 3 independently repeated experiments). (C) The representative immunofluorescence staining images of γH2AX (red) in each group of MIN6 cells. Nuclei were stained with DAPI (blue). Scale bar 50 μm. (D) The quantitative analysis of γH2AX positive cells in different groups (n = 5 independently repeated experiments) Mean ± SEM. $^{*}p < 0.05$, $^{**}p < 0.01$, $^{***}p < 0.001$ indicate significant differences, and *ns* > 0.05 means no significance difference.

Figure. 9. EUG exerted protection of STZ-induced MIN6 cells through inhibition of the apoptosis *in vitro*. (A) The detection of BCL2, BAX, Cleaved Caspase-3 expression in different groups using western blot. (B) The quantification of western blot gel bands in different groups (n = 3 independently repeated experiments). (C) The gene levels of *Bcl2*, *Bax*, and *Bcl2/Bax* in different groups (n = 5 independently repeated experiments). (D) The detection of MIN6 cells apoptosis in each group using TUNEL staining. The cells with red fluorescence represents apoptosis. Scale bar 100 μm. (E) The quantitative analysis of TUNEL positive cells in different groups (n = 5 independently repeated experiments). (F) The apoptosis in each group was analyzed using flow cytometry after Annexin V FITC and PI co-staining. (G) The quantitative analysis of flow cytometry after Annexin V FITC and PI co-staining in different groups (n = 5 independently repeated experiments). Mean ± SEM. $^{*}p < 0.05$, $^{**}p < 0.01$, $^{***}p < 0.001$ indicate significant differences, and *ns* > 0.05 means no significance difference.

Figure. 10. Diagram of the underlying mechanisms involved in the protective effects of EUG on T1DM.

Supplement Figure. 1. EUG alleviated the related complications in T1DM mice. (A) The changes of urine wetting area of bedding material of mice in each group at

different time points were recorded. (B) External appearance and body transformation in each group of mice (n = 5 independently repeated experiments). Scale bar 2 cm. (C) The qualitative determination of urine glucose in each group of mice (n = 5 independently repeated experiments). The shade of orange represents the concentration of glucose in the urine. (D) The PAS staining images of glomerulus paraffin sections in each group of mice. Mean ± SEM. $^{*}p < 0.05$, $^{**}p < 0.01$, $^{***}p < 0.001$ indicate significant differences, and *ns* > 0.05 means no significance difference. Scale bars 50 μm, 20 μm.

Supplement Figure. 2. Statistical map of mRNA differential expression between T1DM group and EUG intervention group. (A) The volcanic map shows the distribution of differential factors. (B) Differential expression cluster heat map, with red indicating up-regulated gene expression and blue indicating down-regulated gene expression. (C-H) GSEA enrichment curve of C: "response to glucose" pathway; D: response to carbohydrate pathway; E: "cellular glucose homeostasis" pathway; F: "positive regulation of insulin secretion" pathway; G: "hydrogen peroxide-mediated programmed cell death" pathway; H: "cellular response to hydrogen peroxide" pathway. The curve represents the cumulative enrichment score (ES), the vertical axis represents the enrichment score, each bar code on the horizontal axis represents a gene, and the color change represents the contribution of that gene to the enrichment score.

Supplement Figure. 3. Explored the optimal concentration of drugs for MIN6 cells *in vitro*. (A) The cell viability of MIN6 treated with different dose STZ for 24 h using CCK-8 assay (n = 5 independently repeated experiments). (B) The safe dose ranges of EUG to maintain cell viability was determined by CCK-8 assay (n = 5 independently repeated experiments). (C) The dose-dependent effect of EUG on MIN6 cell viability after STZ-induced (n = 5 independently repeated experiments). (D) The imaging results of MIN6 cells under an inverted microscope in bright field with different treatments. Scale bars 100 μm. Mean ± SEM. $^{*}p < 0.05$, $^{**}p < 0.01$, $^{***}p <$

0.001 indicate significant differences, and *ns* > 0.05 means no significance difference.

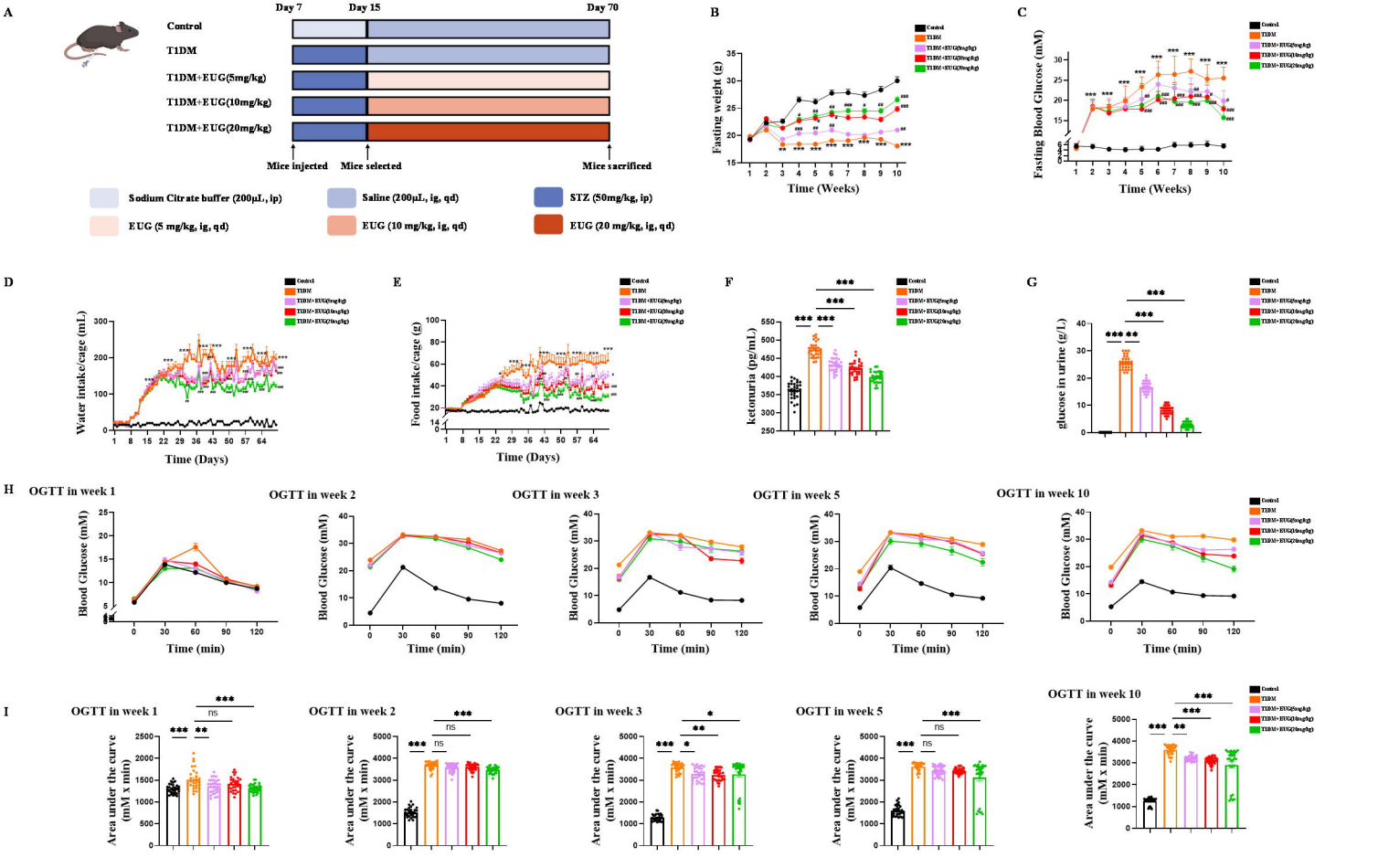
A
Day 7
Day 15
Day 70
Control
T1DM
T1DM+EUG(5mg/kg)
T1DM+EUG(10mg/kg)
T1DM+EUG(20mg/kg)
Mice injected
Mice selected
Mice sacrificed
Sodium Citrate buffer (200μL, ip)
Saline (200μL, ig, qd)
STZ (50mg/kg, ip)
EUG (5 mg/kg, ig, qd)
EUG (10 mg/kg, ig, qd)
EUG (20 mg/kg, ig, qd)
B
Fasting weight (g)
Time (Weeks)
C
Fasting Blood Glucose (mM)
Time (Weeks)
D
Water intake/cage (mL)
Time (Days)
E
Food intake/cage (g)
Time (Days)
F
ketonuria (pg/mL)
G
glucose in urine (g/L)
H
OGTT in week 1
OGTT in week 2
OGTT in week 3
OGTT in week 5
OGTT in week 10
Blood Glucose (mM)
Time (min)
I
OGTT in week 1
OGTT in week 2
OGTT in week 3
OGTT in week 5
OGTT in week 10
Area under the curve (mM x min)

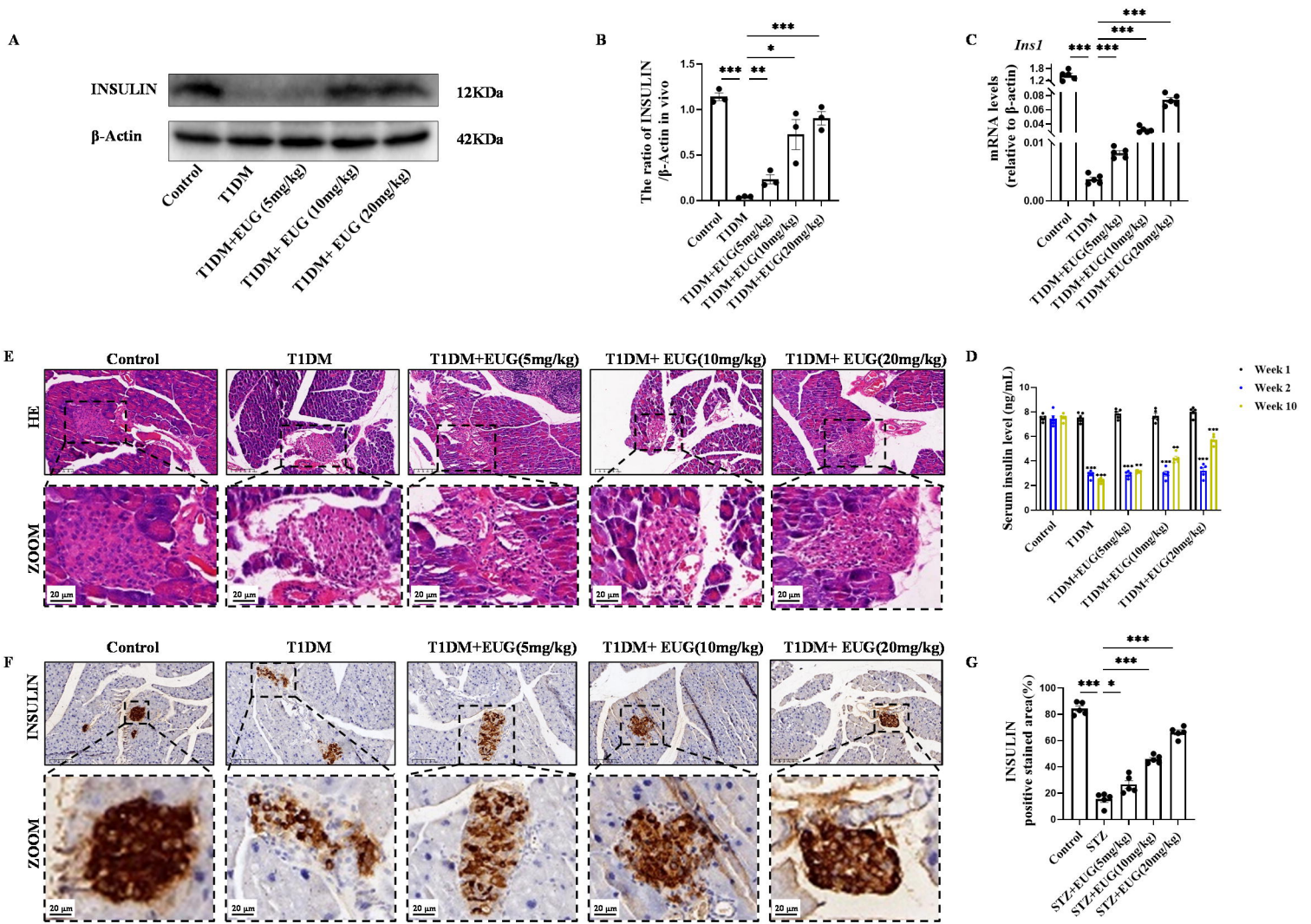
A
INSULIN
β-Actin
12KDa
42KDa
Control
T1DM
T1DM+EUG (5mg/kg)
T1DM+ EUG (10mg/kg)
T1DM+ EUG (20mg/kg)
B
The ratio of INSULIN /β-Actin in vivo
C
Ins1
mRNA levels (relative to β-actin)
D
Serum insulin level (ng/mL)
Week 1
Week 2
Week 10
E
HE
ZOOM
20 μm
F
INSULIN
G
INSULIN positive stained area(%)
STZ
STZ+EUG(5mg/kg)
STZ+EUG(10mg/kg)
STZ+EUG(20mg/kg)

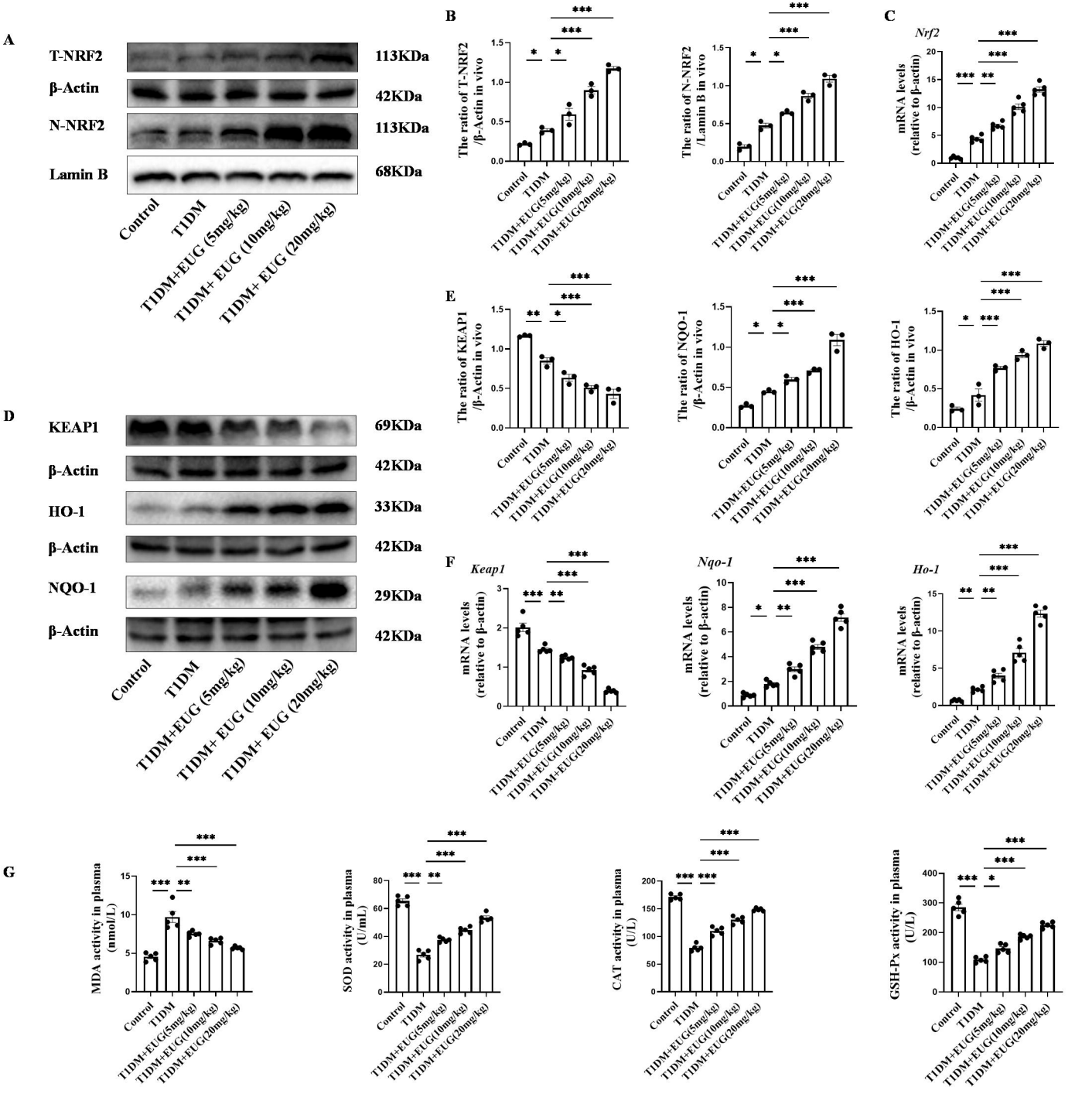
A
T-NRF2
β-Actin
N-NRF2
Lamin B
113KDa
42KDa
113KDa
68KDa
Control
T1DM
T1DM+EUG (5mg/kg)
T1DM+ EUG (10mg/kg)
T1DM+ EUG (20mg/kg)
B
The ratio of T-NRF2 /β-Actin in vivo
The ratio of N-NRF2 /Lamin B in vivo
C
Nrf2
mRNA levels (relative to β-actin)
D
KEAP1
β-Actin
HO-1
NQO-1
69KDa
42KDa
33KDa
42KDa
29KDa
42KDa
E
The ratio of KEAP1 /β-Actin in vivo
The ratio of NQO-1 /β-Actin in vivo
The ratio of HO-1 /β-Actin in vivo
F
Keap1
Nqo-1
Ho-1
mRNA levels (relative to β-actin)
G
MDA activity in plasma (nmol/L)
SOD activity in plasma (U/mL)
CAT activity in plasma (U/L)
GSH-Px activity in plasma (U/L)
T1DM+EUG(5mg/kg)
T1DM+EUG(10mg/kg)
T1DM+EUG(20mg/kg)

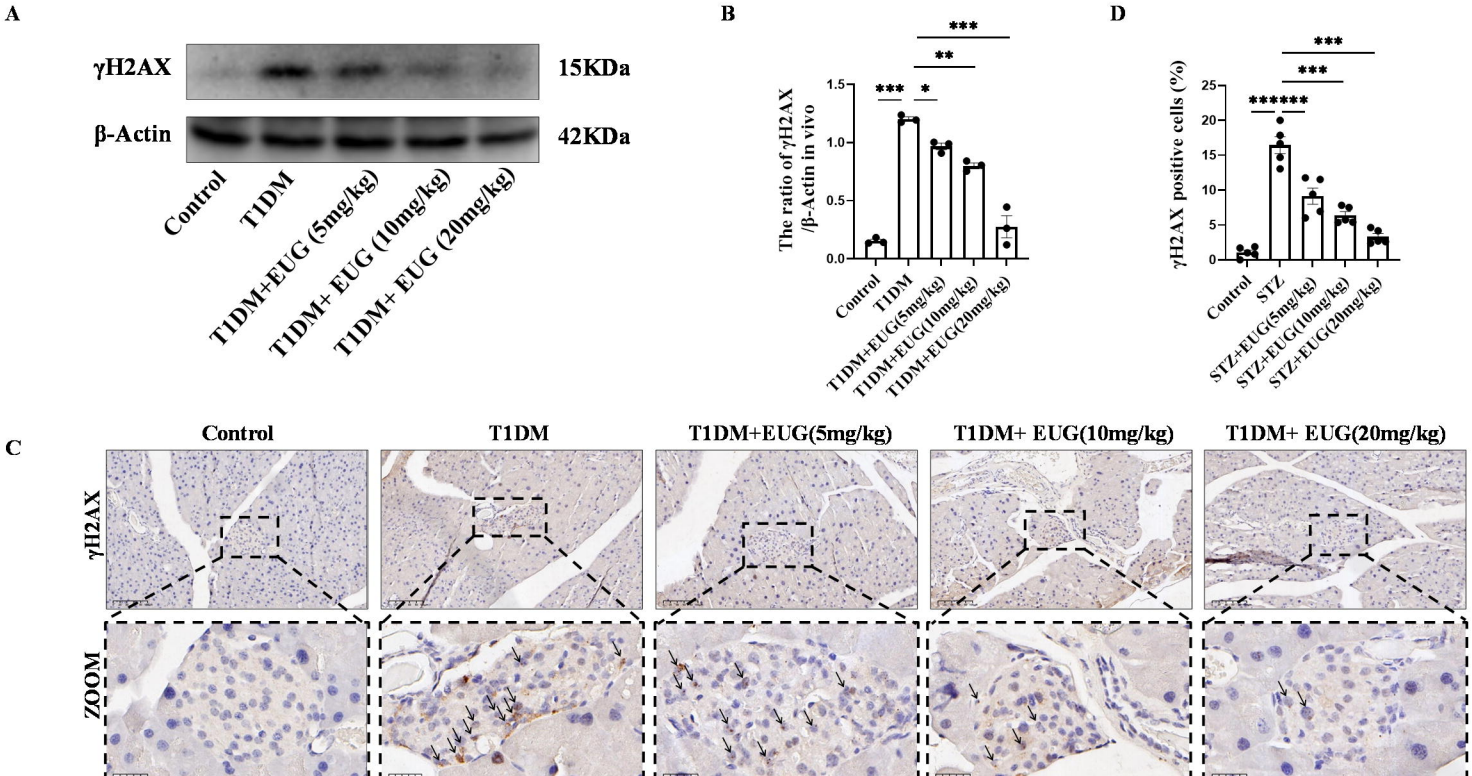
A
γH2AX
15KDa
β-Actin
42KDa
Control
T1DM
T1DM+EUG (5mg/kg)
T1DM+ EUG (10mg/kg)
T1DM+ EUG (20mg/kg)
B
The ratio of γH2AX /β-Actin in vivo
1.5
1.0
0.5
0.0
***
*
**
***
Control
T1DM
T1DM+EUG(5mg/kg)
T1DM+EUG(10mg/kg)
T1DM+EUG(20mg/kg)
D
γH2AX positive cells (%)
25
20
15
10
5
0
****
***
***
Control
STZ
STZ+EUG(5mg/kg)
STZ+EUG(10mg/kg)
STZ+EUG(20mg/kg)
C
Control
T1DM
T1DM+EUG(5mg/kg)
T1DM+ EUG(10mg/kg)
T1DM+ EUG(20mg/kg)
γH2AX
ZOOM

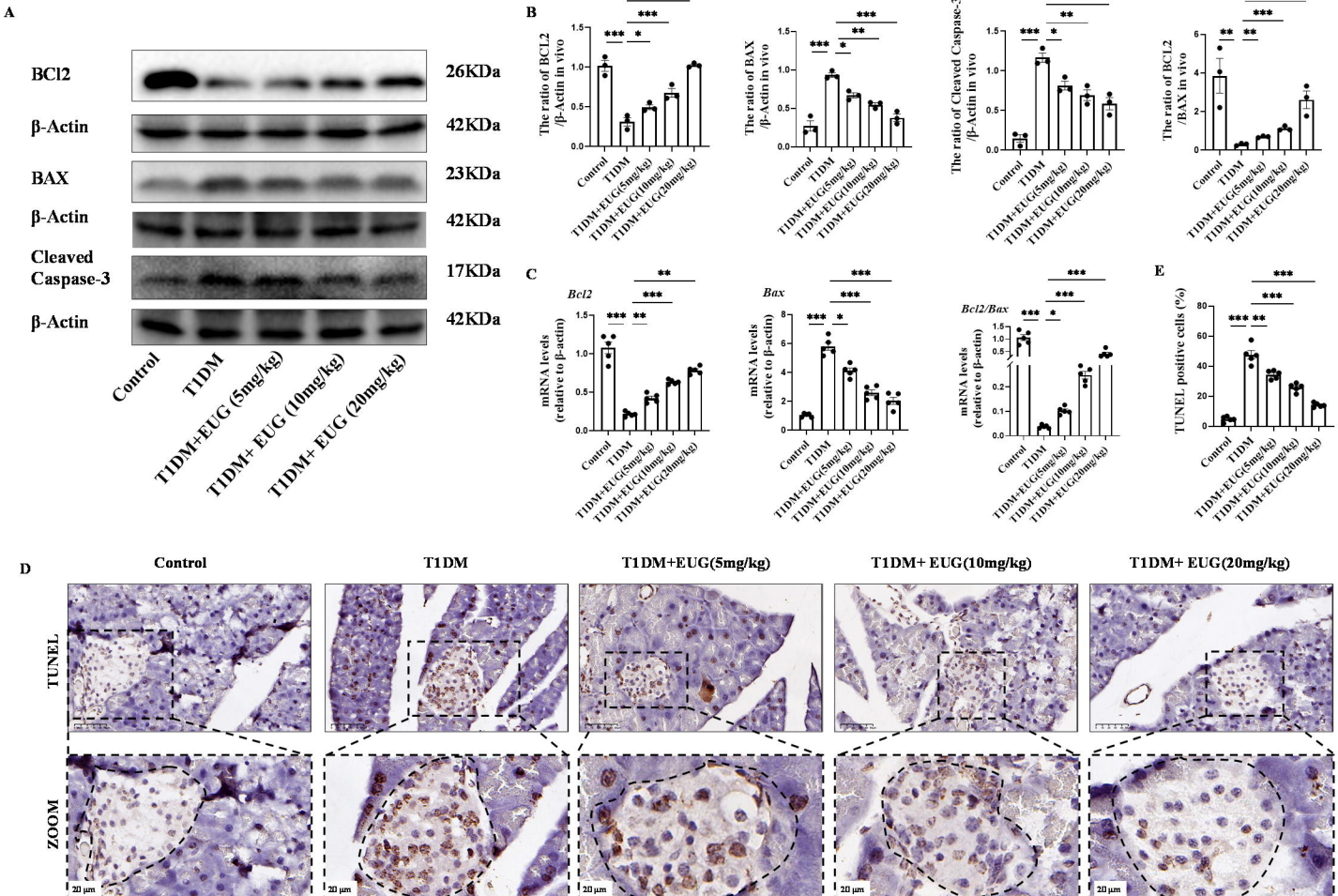
A
BCl2
β-Actin
BAX
β-Actin
Cleaved Caspase-3
β-Actin
26KDa
42KDa
23KDa
42KDa
17KDa
42KDa
Control
T1DM
T1DM+EUG (5mg/kg)
T1DM+ EUG (10mg/kg)
T1DM+ EUG (20mg/kg)
B
The ratio of BCL2 /β-Actin in vivo
The ratio of BAX /β-Actin in vivo
The ratio of Cleaved Caspase-3 /β-Actin in vivo
The ratio of BCL2 /BAX in vivo
C
Bcl2
Bax
Bcl2/Bax
mRNA levels (relative to β-actin)
E
TUNEL positive cells (%)
D
Control
T1DM
T1DM+EUG(5mg/kg)
T1DM+ EUG(10mg/kg)
T1DM+ EUG(20mg/kg)
TUNEL
ZOOM
20 μm

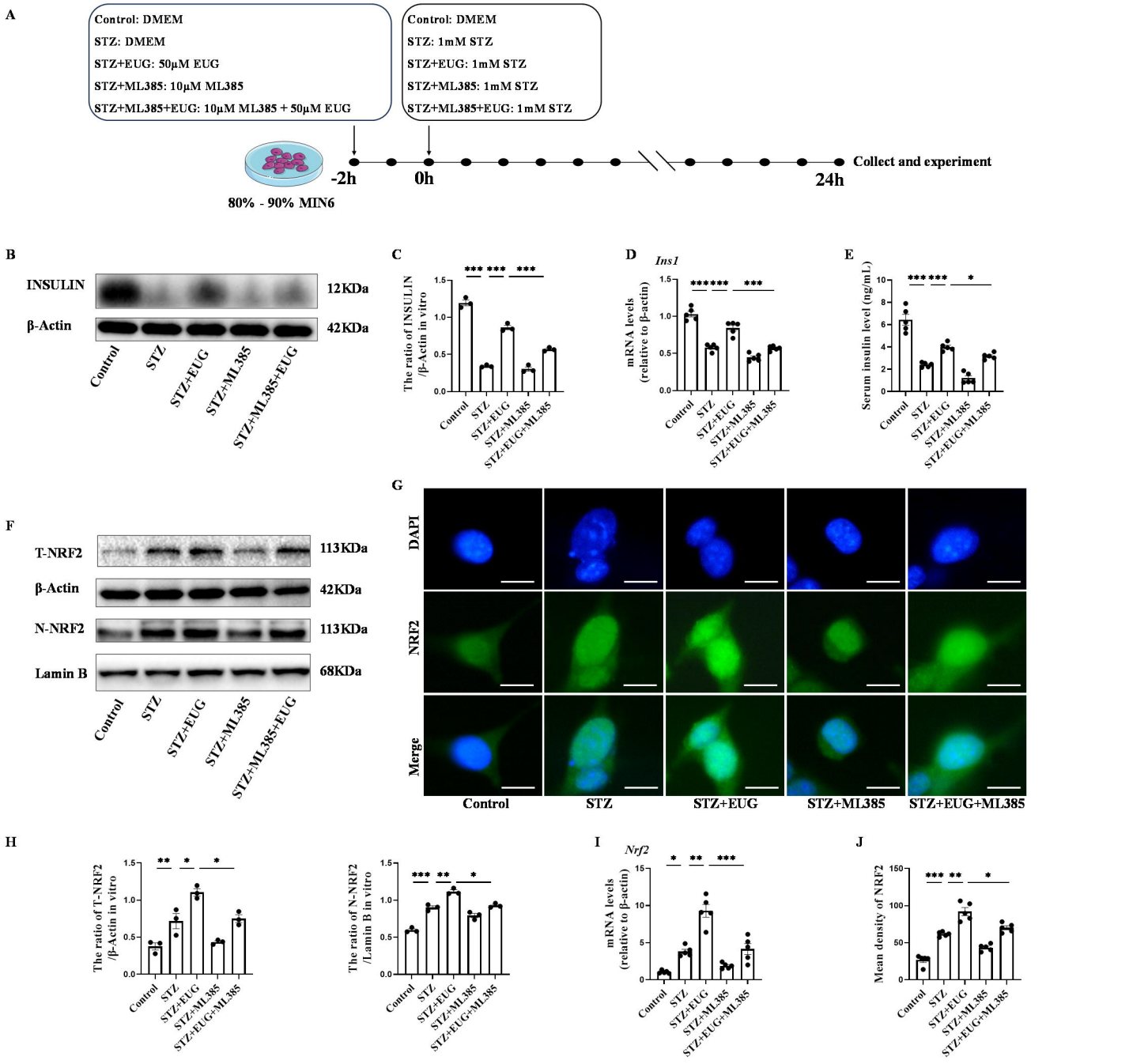
A
Control: DMEM
STZ: DMEM
STZ+EUG: 50μM EUG
STZ+ML385: 10μM ML385
STZ+ML385+EUG: 10μM ML385 + 50μM EUG
Control: DMEM
STZ: 1mM STZ
STZ+EUG: 1mM STZ
STZ+ML385: 1mM STZ
STZ+ML385+EUG: 1mM STZ
-2h
0h
24h
Collect and experiment
80% - 90% MIN6
B
INSULIN
β-Actin
12KDa
42KDa
Control
STZ
STZ+EUG
STZ+ML385
STZ+ML385+EUG
C
The ratio of INSULIN /β-Actin in vitro
D
Ins1
mRNA levels (relative to β-actin)
E
Serum insulin level (ng/mL)
F
T-NRF2
β-Actin
N-NRF2
Lamin B
113KDa
42KDa
113KDa
68KDa
G
DAPI
NRF2
Merge
Control
STZ
STZ+EUG
STZ+ML385
STZ+EUG+ML385
H
The ratio of T-NRF2 /β-Actin in vitro
The ratio of N-NRF2 /Lamin B in vitro
I
Nrf2
mRNA levels (relative to β-actin)
J
Mean density of NRF2

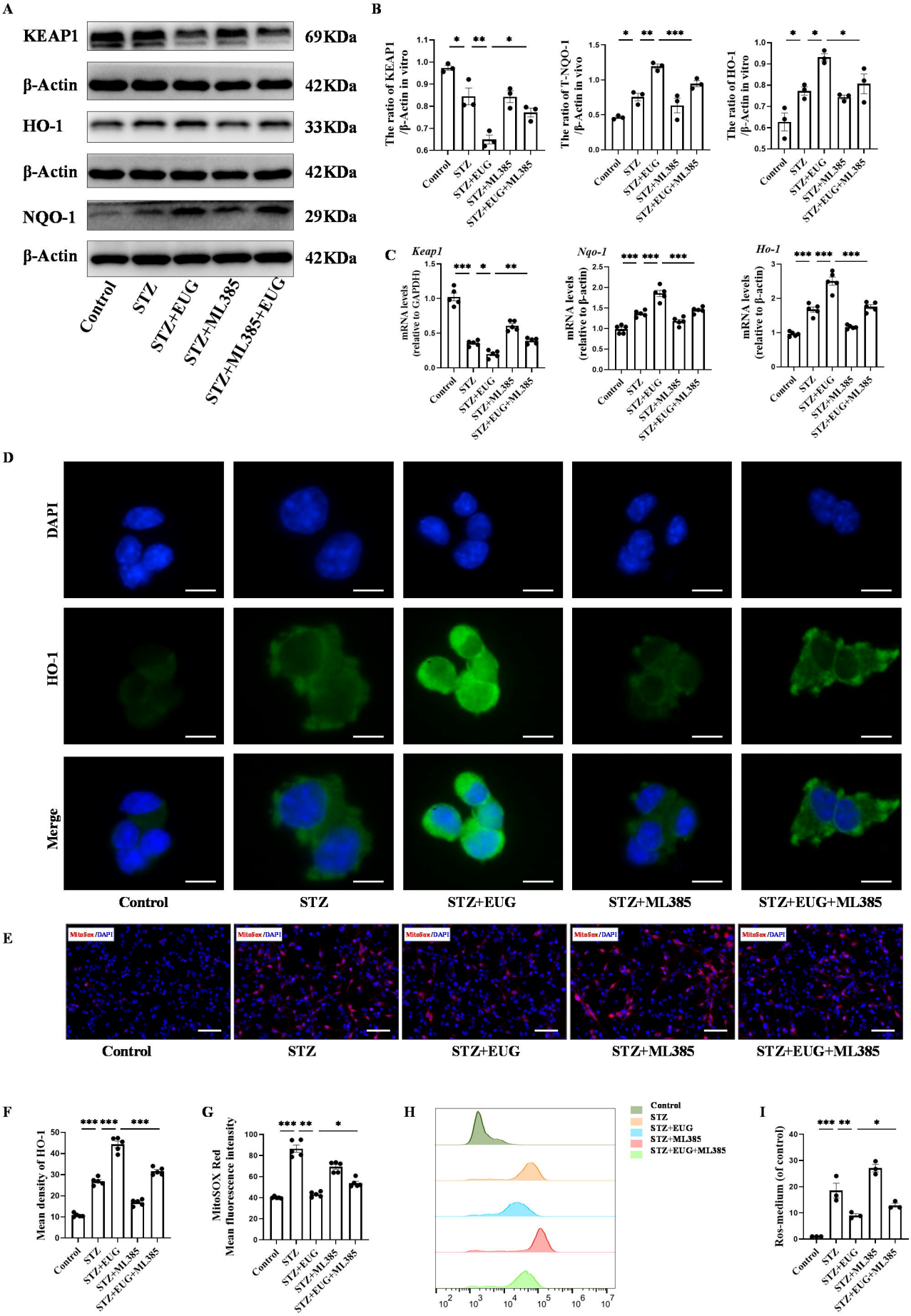
A
KEAP1
69KDa
β-Actin
42KDa
HO-1
33KDa
β-Actin
42KDa
NQO-1
29KDa
β-Actin
42KDa
Control
STZ
STZ+EUG
STZ+ML385
STZ+ML385+EUG
B
The ratio of KEAP1 /β-Actin in vitro
The ratio of T-NQO-1 /β-Actin in vivo
The ratio of HO-1 /β-Actin in vitro
C
Keap1
Nqo-1
Ho-1
mRNA levels (relative to GAPDH)
mRNA levels (relative to β-actin)
D
DAPI
HO-1
Merge
Control
STZ
STZ+EUG
STZ+ML385
STZ+EUG+ML385
E
MitoSox /DAPI
Control
STZ
STZ+EUG
STZ+ML385
STZ+EUG+ML385
F
Mean density of HO-1
G
MitoSOX Red Mean fluorescence intensity
H
Control
STZ
STZ+EUG
STZ+ML385
STZ+EUG+ML385
I
Ros-medium (of control)

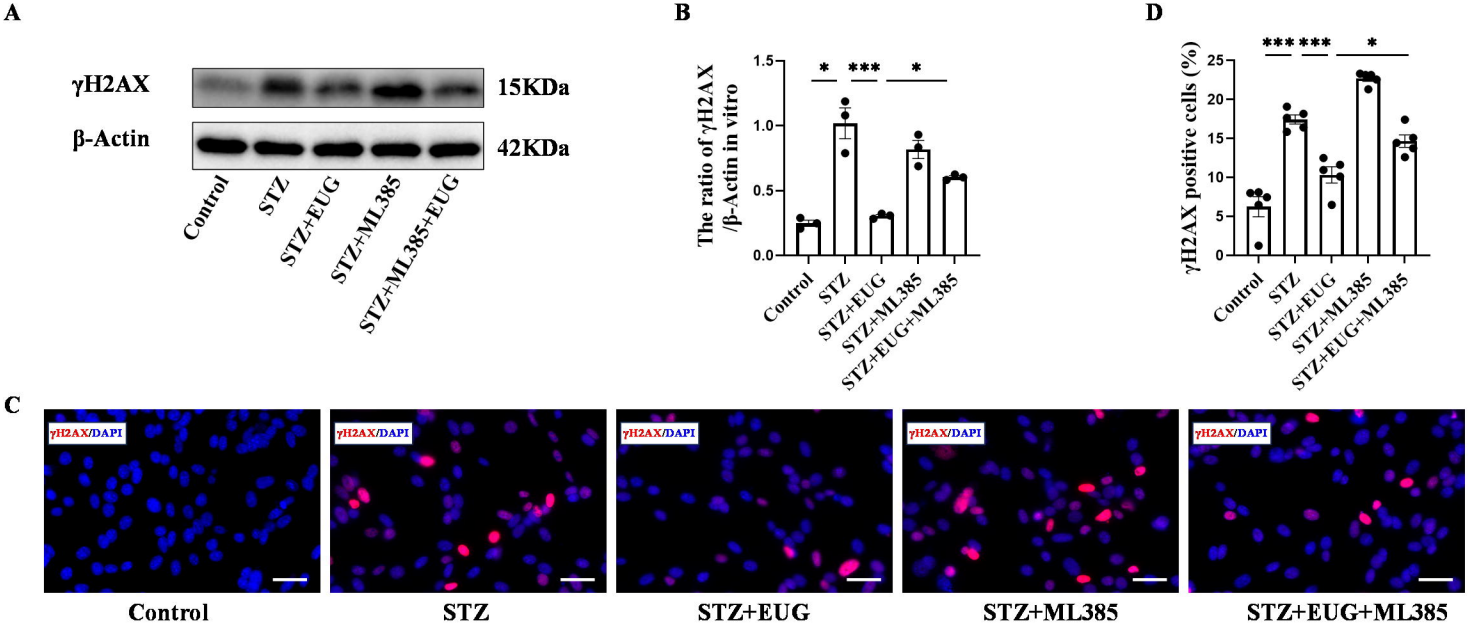
A
γH2AX
β-Actin
15KDa
42KDa
Control
STZ
STZ+EUG
STZ+ML385
STZ+ML385+EUG
B
The ratio of γH2AX /β-Actin in vitro
1.5
1.0
0.5
0.0
*
***
*
Control
STZ
STZ+EUG
STZ+ML385
STZ+EUG+ML385
D
γH2AX positive cells (%)
25
20
15
10
5
0
***
***
*
Control
STZ
STZ+EUG
STZ+ML385
STZ+EUG+ML385
C
γH2AX/DAPI
Control
STZ
STZ+EUG
STZ+ML385
STZ+EUG+ML385

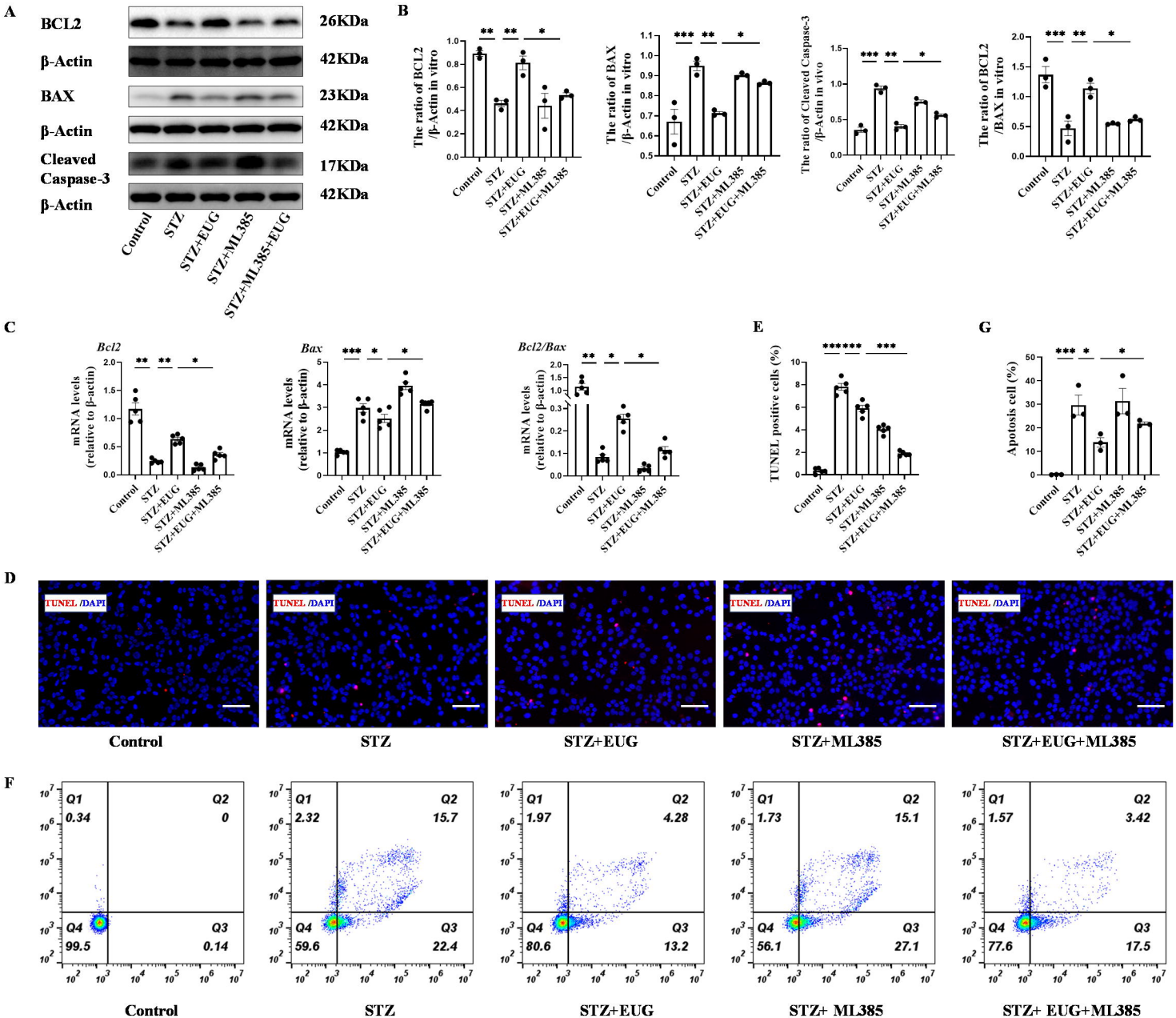
A
BCL2
26KDa
β-Actin
42KDa
BAX
23KDa
β-Actin
42KDa
Cleaved Caspase-3
17KDa
β-Actin
42KDa
Control
STZ
STZ+EUG
STZ+ML385
STZ+ML385+EUG
B
The ratio of BCL2 /β-Actin in vitro
The ratio of BAX /β-Actin in vitro
The ratio of Cleaved Caspase-3 /β-Actin in vivo
The ratio of BCL2 /BAX in vitro
C
Bcl2
Bax
Bcl2/Bax
mRNA levels (relative to β-actin)
E
TUNEL positive cells (%)
G
Apoptosis cell (%)
D
TUNEL /DAPI
Control
STZ
STZ+EUG
STZ+ML385
STZ+EUG+ML385
F
Q1 0.34
Q2 0
Q4 99.5
Q3 0.14
Q1 2.32
Q2 15.7
Q4 59.6
Q3 22.4
Q1 1.97
Q2 4.28
Q4 80.6
Q3 13.2
Q1 1.73
Q2 15.1
Q4 56.1
Q3 27.1
Q1 1.57
Q2 3.42
Q4 77.6
Q3 17.5
Control
STZ
STZ+EUG
STZ+ ML385
STZ+ EUG+ML385

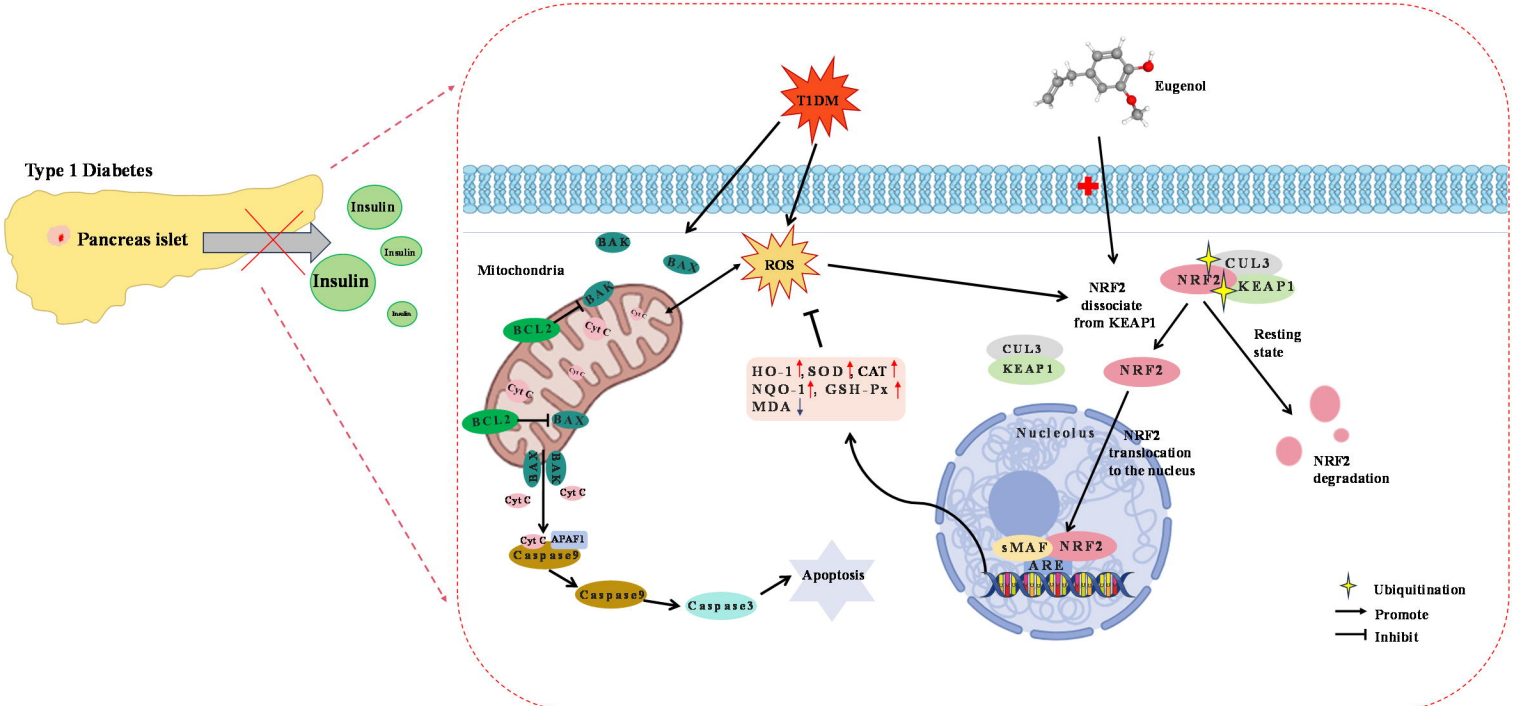
Type 1 Diabetes
Pancreas islet
Insulin
Insulin
Insulin
Insulin
T1DM
Eugenol
BAK
BAX
Mitochondria
ROS
BAK
BCL2
Cyt C
Cyt C
Cyt C
BCL2
BAX
BAX
BAX
Cyt C
Cyt C
Cyt C
APAF1
Caspase9
Caspase9
Caspase3
Apoptosis
HO-1↑, SOD↑, CAT↑
NQO-1↑, GSH-Px↑
MDA↓
NRF2
dissociate
from KEAP1
CUL3
NRF2
KEAP1
Resting
state
CUL3
KEAP1
NRF2
Nucleolus
NRF2
translocation
to the nucleus
NRF2
degradation
sMAF
NRF2
ARE
Ubiquitination
Promote
Inhibit

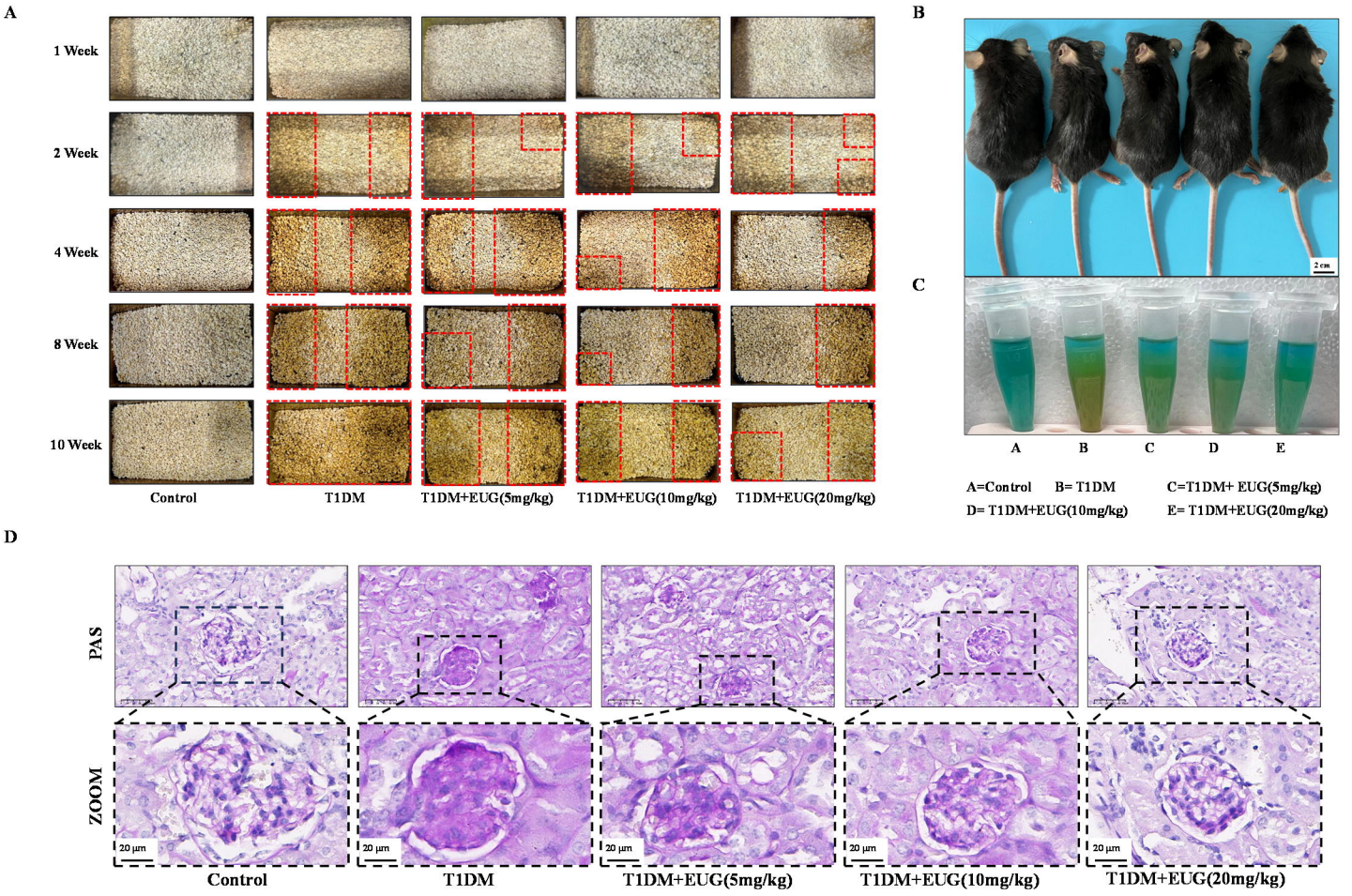
A
1 Week
2 Week
4 Week
8 Week
10 Week
Control
T1DM
T1DM+EUG(5mg/kg)
T1DM+EUG(10mg/kg)
T1DM+EUG(20mg/kg)
B
2 cm
C
A
B
C
D
E
A=Control B= T1DM C=T1DM+ EUG(5mg/kg)
D= T1DM+EUG(10mg/kg) E= T1DM+EUG(20mg/kg)
D
PAS
ZOOM
20 μm
Control
T1DM
T1DM+EUG(5mg/kg)
T1DM+EUG(10mg/kg)
T1DM+EUG(20mg/kg)

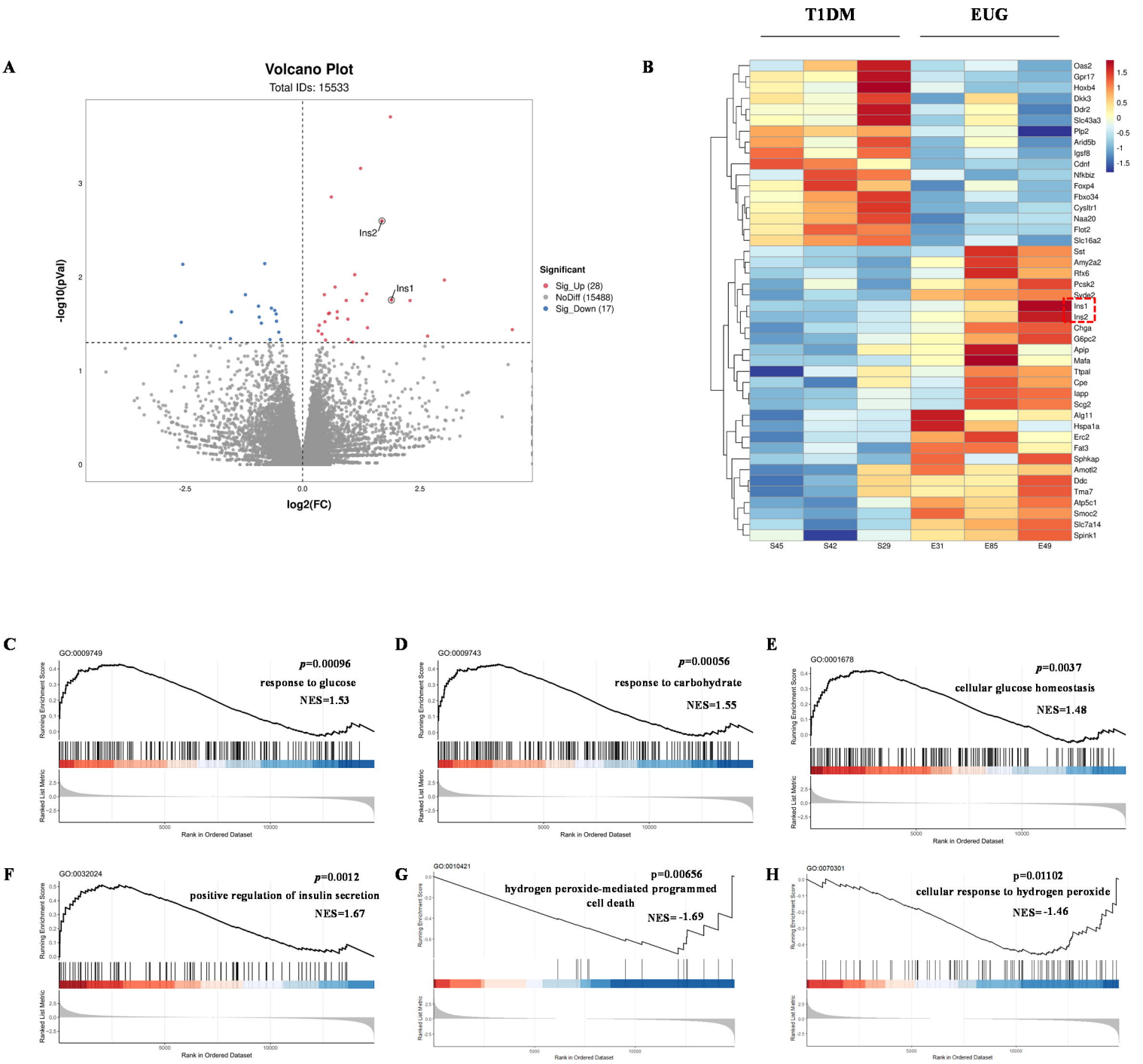
A
Volcano Plot
Total IDs: 15533
-log10(pVal)
log2(FC)
Ins2
Ins1
Significant
Sig_Up (28)
NoDiff (15488)
Sig_Down (17)
B
T1DM
EUG
Oas2
Gpr17
Hoxb4
Dkk3
Ddr2
Slc43a3
Plp2
Arid5b
Igsf8
Cdnf
Nfkbiz
Foxp4
Fbxo34
Cysltr1
Naa20
Flot2
Slc16a2
Sst
Amy2a2
Rfx6
Pcsk2
Syde2
Ins1
Ins2
Chga
G6pc2
Apip
Mafa
Ttpal
Cpe
Iapp
Scg2
Alg11
Hspa1a
Erc2
Fat3
Sphkap
Amotl2
Ddc
Tma7
Atp5c1
Smoc2
Slc7a14
Spink1
S45
S42
S29
E31
E85
E49
C
GO:0009749
p=0.00096
response to glucose
NES=1.53
D
GO:0009743
p=0.00056
response to carbohydrate
NES=1.55
E
GO:0001678
p=0.0037
cellular glucose homeostasis
NES=1.48
F
GO:0032024
p=0.0012
positive regulation of insulin secretion
NES=1.67
G
GO:0010421
p=0.00656
hydrogen peroxide-mediated programmed cell death
NES= -1.69
H
GO:0070301
p=0.01102
cellular response to hydrogen peroxide
NES= -1.46
Running Enrichment Score
Ranked List Metric
Rank in Ordered Dataset

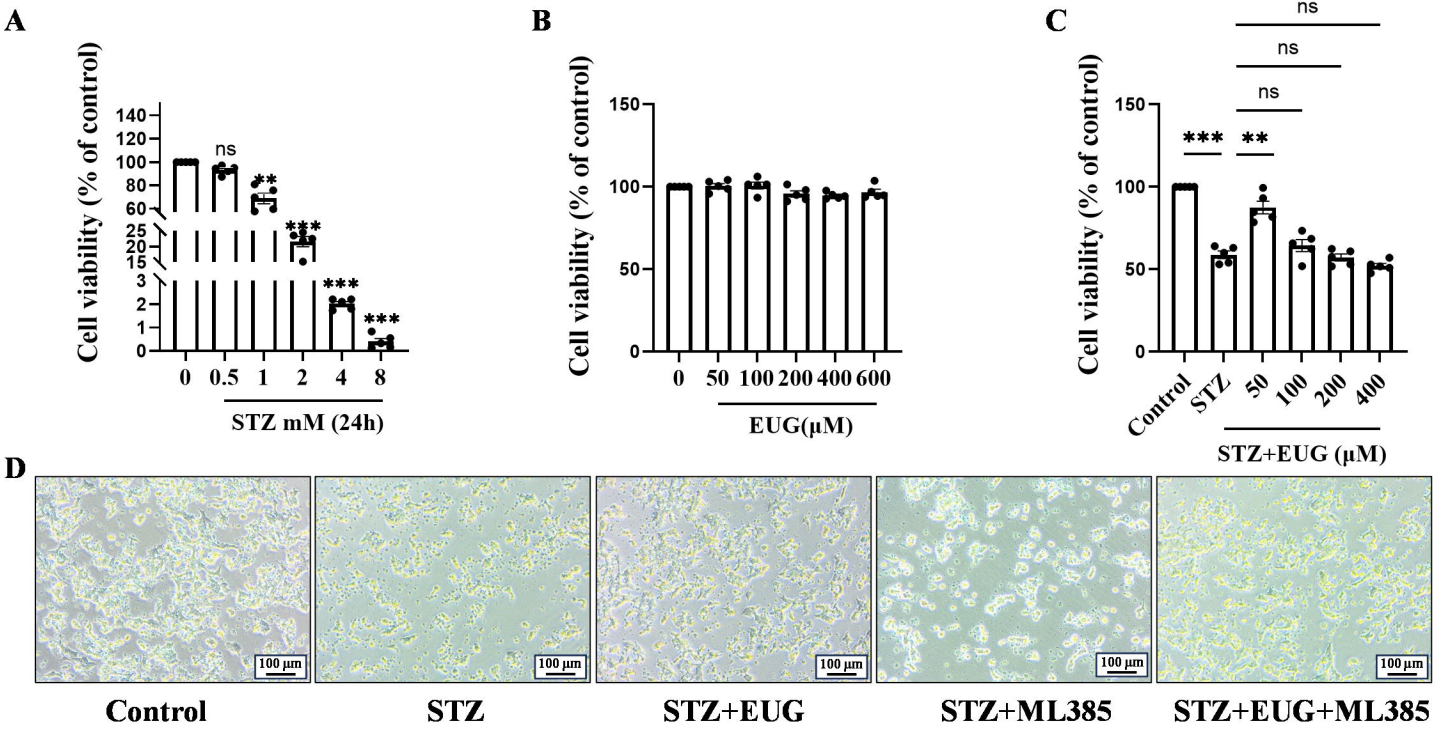
A
Cell viability (% of control)
140
120
100
80
60
25
20
15
3
2
1
0
ns
**
***
***
***
0
0.5
1
2
4
8
STZ mM (24h)
B
Cell viability (% of control)
150
100
50
0
0
50
100
200
400
600
EUG(μM)
C
Cell viability (% of control)
150
100
50
0
ns
ns
ns
***
**
Control
STZ
50
100
200
400
STZ+EUG (μM)
D
100 μm
Control
STZ
STZ+EUG
STZ+ML385
STZ+EUG+ML385